NASA Contractor Report 189102

Materials Technology for Stirling Space Power Converters

William Baggenstoss and Donald Mittendorf
Allied-Signal Aerospace Company
Garrett Fluid Systems Division
1300 W. Warner Road
Tempe, Arizona 85284

July 1992

Date for general release July 1994

Prepared for
Lewis Research Center
Under Contract NAS3-26065

National Aeronautics and
Space Administration

TABLE OF CONTENTS

LIST OF FIGURES

LIST OF TABLES

1. SUMMARY

This program on Materials Technology for Stirling Space Power Converters was conducted in support of the NASA Lewis Research Center development of the Stirling power converter (SPC) for space power applications. The objectives of this contract were 1) to perform a technology review and analyses to support the evaluation of materials issues for the SPC; 2) to evaluate liquid metal compatibility issues of the SPC; 3) to evaluate and define a transient liquid-phase diffusion-bonding (TLPDB) process for the SPC joints to the Udimet 720 heater head; and 4) to evaluate alternative (to the TLPDB) joining techniques.

In the technology review, several aspects of the current Stirling design were examined: specifically, the assembly process and materials joining, the displacer and piston gas bearings, and the power converter heat exchangers. In addition, alternative design concepts were generated including a passive hydrodynamic bearing, a concentric tube cooler, and alternative heater head fabrication methods. The supporting analyses included GLIMPS power converter simulation in support of the materials studies, and system-level analysis in support of the technology review. The system level analysis showed that Stirling systems with the configuration defined by NASA Lewis optimize at a temperature ratio of around 1.9 and display high system mass sensitivity to temperature ratio. The liquid metal compatibility study evaluated the use of liquid lithium, liquid sodium, and liquid NaK in the Stirling power converter. The analysis showed that the use of liquid lithium will require the use of refractory alloys, while the use of liquid sodium and NaK with superalloys should be acceptable with careful design. The TLPDB study developed specific TLPDB process parameters for use in the Stirling power converter. The alternative joining techniques study looked at the applicability of various joining techniques to the Stirling power converter requirements. The results of the study showed that TLPDB has the lowest risk for the Udimet 720 joints, with electron beam (EB) welding being a higher risk alternative.

Based on the technology review, it is recommended that changes in the power converter assembly sequence be incorporated to facilitate the use of TLPDB. In addition, it is recommended that further examination of alternative design concepts for the power converter bearings and heat exchangers be undertaken. The liquid metal study indicates that compatibility testing should be performed under conditions which simulate expected operational systems as closely as possible. The TLPDB study shows that the technique can be applied to many joints in the Stirling power converter. Based on the alternative joining techniques study, TLPDB is recommended for all Udimet 720 joints. This program was limited to a theoretical evaluation of the TLPDB process for the Stirling power converter. It is recommended that the next step in the development of TLPDB for this application be demonstration of the process on sample coupons, prior to applying TLPDB to actual power converter hardware.

2. INTRODUCTION

This report, prepared by Garrett Fluid Systems Division (GFSD), Tempe, Arizona, is submitted to NASA Lewis Research Center, Cleveland, Ohio. It has been prepared in compliance with the requirements of the statement of work (SOW) contained in Purchase Order NAS3-26065 and is the final report for work performed in accordance with the above referenced SOW.

The ongoing NASA Stirling engine program has made substantial progress in the development of the Stirling power converters for space power applications. This effort is part of the NASA Civil Space Technology Initiative (CSTI) High Capacity Power Project (reference 1). Current Stirling development efforts by NASA Lewis and its main contractor Mechanical Technology Incorporated (MTI) are focusing on several key power converter subsystems, and in each case there are significant materials issues to be resolved. Two important materials issues are liquid metal compatibility and metal joining, and these were the main focus of this program on Materials Technology for Stirling Space Power Converters.

The liquid metal compatibility issue comes into play at three locations: the hot-end heat exchanger, the cold-end heat exchanger, and in the reactor loop. The liquid metals currently planned to be used are sodium, NaK, and lithium respectively. The effect of liquid metal corrosion on the strength of the component materials is important in all three cases. In addition, because the required system life is very long for space power applications, fatigue/creep issues are critical. Therefore, the effect of liquid metal exposure to material fatigue/creep properties must be evaluated to ensure that the materials used will have acceptable long-term performance. The liquid metal compatibility study examined the use of liquid sodium, NaK, and lithium in the Stirling power converter.

Metal joining presents challenges in a Stirling power converter for space applications. To meet the long life requirements of space power converters, a high-strength superalloy, Udimet 720, has been selected for the Stirling heater head; the high-strength superalloys cannot normally be joined by standard fusion welding techniques. In addition, the requirements for heater head joints are quite severe. First, the joints must contain the helium working fluid in the power converter which operates at high, varying pressures. Next, because of critical dimensional relationships within the power converter, the metal joining process must not distort the housing. This is made more difficult by the fact that the housing is as thin as possible to keep system weight low. Due to the high operating pressure of the power converter, the housing joints must retain high strength properties, particularly fatigue/creep resistance. In addition, due to the high reliability required of space power systems, the metal joints must be inspectable. TLPDB is well suited to the requirements of the Stirling power converter application because it can yield very low distortion, high strength, inspectable joints. A TLPDB process for the Stirling power converter was defined as part of this program. Other metal joining techniques were also evaluated for their applicability to the Stirling power converter applications.

To prepare for the materials studies and to generate potential new concepts, a Stirling technology review was conducted. In addition, power converter and system level analyses were performed to support the technology review and materials studies efforts. Presentation of the work performed on the program is divided into three main sections: the Technology Review, Supporting Analysis, and the Materials Studies.

3. TECHNOLOGY REVIEW

3.1 Heater Head Assembly Sequence Using TLPDB

3.1.1 Assembly Sequence Analysis

The first step in the analysis of the heater head assembly sequence was to develop an approach to evaluate the assembly in concert with the materials joining study. The following method was developed:

1. Identify materials for each joint
2. Identify stress levels for each joint
3. Identify materials joining options
4. Establish preliminary assembly process steps
5. Determine if the joining option at each process step is
   a) Compatible with materials and sub-assemblies from previous steps
   b) Meets the joint design drivers and requirements
6. Modify process steps and/or joining options based on results of step 5
7. Establish recommended assembly process steps

Joint stress levels were a key factor in this effort. Because the joining process that could be used was dependent on the stress levels, and the assembly sequence is highly dependent on the joining process, the entire assembly sequence was dependent on the joint stress requirements. The pertinent stress data for this study was provided by MTI.

Changes were made to the assembly sequence as the NASA/MTI power converter design evolved. MTI changed from two heat treats in the Udimet 720 portion of the power converter to a single heat treat, and the location of the transition point from the Udimet 720 to the Inconel 718 was changed during the course of the program.

The study of the heater head assembly sequence not only provided results for the technology review, but was also used as an input to the materials joining techniques study.

3.1.2 Assembly Sequence Results

The location of the joints in the heater head of the power converter are shown in Figure 1. (For the long-life power converter, joint 6 will replace the O-rings shown in Figure 1.) After several iterations, the final assembly sequence developed was as follows:

1. Block of Udimet 720

2. Rough machine

3. Electrical discharge machine (EDM) fins in heater head

4. Chemical mill to remove recast layer

5. STEM drill holes in heater head fins

6. Start diffusion bond of joint 4, regenerator outer wall to heater head. This is a short temperature cycle to initiate the bonding of this joint.

7. Clean-up machine joint 4 surfaces as required.

8. Assemble heater head, heat pipe flanges, regenerator, and cooler.

   *There will be self-fixturing features on heater head for joints 2, 3, and joint 7 (heat pipe flanges).

   *Joint 7 consists of thin Inconel 718 flanges TLPD bonded to the Udimet 720 portion of the heater head. The Inconel 718 heat pipe portion of the heater head can then be TIG welded to the Inconel 718 flanges (step 10).

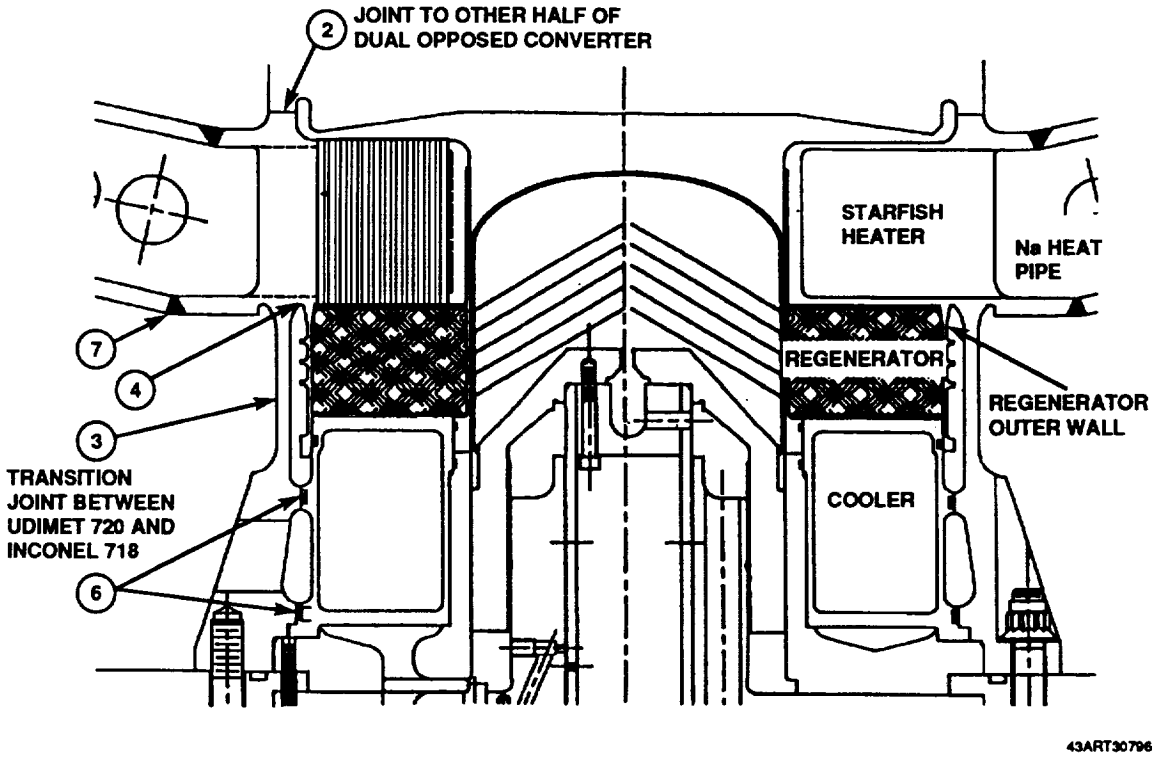

Figure 1. Joint Locations in Stirling Power Converter Heater Head

* A single diffusion-bonding temperature/load cycle bonds:
- axial joints 2 and 3
- radial joints 6 (if required) and 7 (the load for these joints will be provided by interference fits).

*The thermal cycle for the second bond will also complete the diffusion profile for joint 4.

9. Clean-up machine joint 7 flanges, all self-fixturing features, and heater head outside diameter. The outside diameter of the heater head outer wall will be thicker than its final dimension to provide the same joint load during bonding for all joints.

10. Join 718 heat pipe to heater head with TIG weld (joint 7).

11. Fill system with sodium and optimize sodium charge (may require one or more hydrogen fires to 1750 °F followed by vacuum bake out at 1750 °F to remove oxygen before filling with sodium).

12. Final heat treat.

13. Clean-up machine heater head inside diameter.

A Kalrez O-ring is used in the current design at the regenerator outer wall/cooler shell interface. This O-ring could not survive diffusion bonding temperatures. Other concerns over the use of Kalrez seals in a flight power converter existed:

a) Kalrez seals would not survive the required 60,000 hour life at the relatively high Stirling power converter operating temperature,

b) Leak testing of a Kalrez seal at the regenerator outer wall would be difficult,

c) If a Kalrez seal at the regenerator outer wall were found to have a leak, replacement of the seal would be very difficult with a bonded power converter design, and

d) In a bonded power converter design, additional complexity would have to be added to the bonding process to allow the use of a Kalrez seal.

Several concepts were examined to avoid the problem of Kalrez seals being incompatible with a bonded power converter design. The first idea was to bond the regenerator outer wall to the cooler and to use a bellows concept for the regenerator outer wall to handle higher stresses (see Figure 2). Other solutions considered were:

a) Using a carbon, graphite, or ceramic seal,

b) Filling the dead space between the regenerator outer wall and the power converter housing with ceramic foam or ring (to reduce the amount of dead space that would be added to the regenerator in the event of a leak), and

c) Modifying the assembly sequence to end with a weld allowing the use of a Kalrez seal. (This would resolve only the assembly issue, but would not address the other concerns).

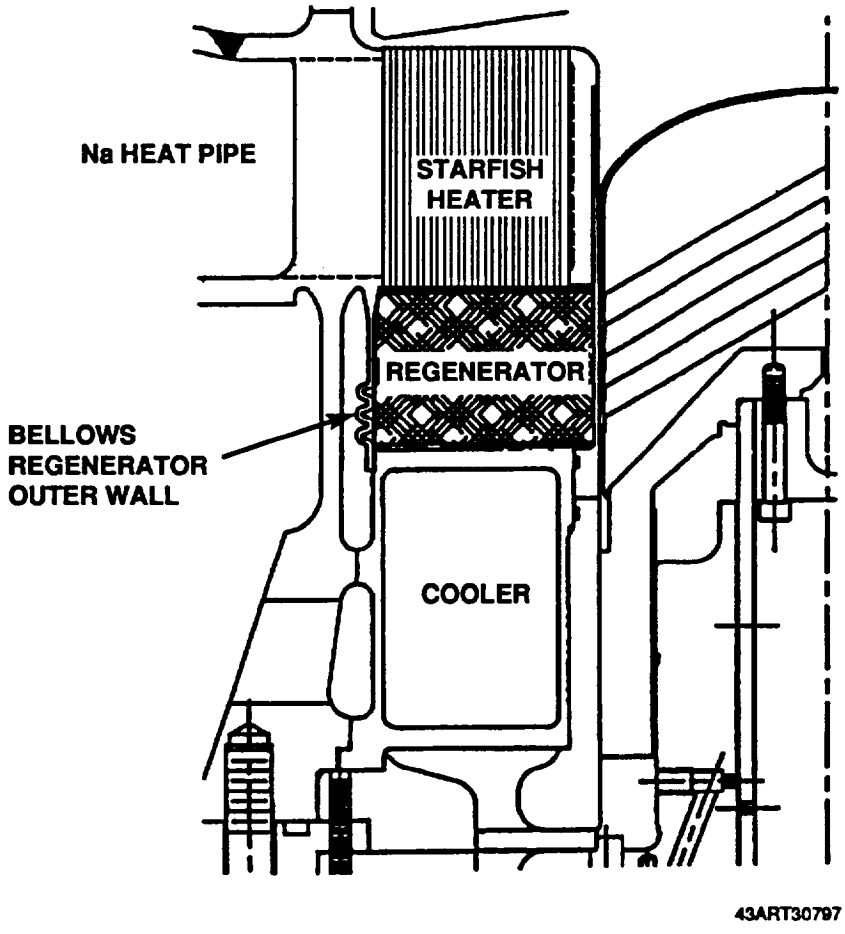

Figure 2. Bellows Regenerator Outer Wall Concept

A solution offered by MTI was to overlap the regenerator wall and cooler wall, without a seal. (This would require special steps to avoid bonding in a bonded power converter design.)

3.1.3 Assembly Sequence Conclusions/Recommendations

It is recommended that the assembly sequence presented above, utilizing TLPDB, be used and that Kalrez seals not be used in a flight design.

3.2 Bearings

3.2.1 Bearings Analysis

The current NASA/MTI Stirling power converter design uses hydrostatic bearings to support the piston and the displacer. The design operates by maintaining a high-pressure supply to feed the bearings and low-pressure reservoirs for gas recovery. This function is provided by a somewhat complex system of ports and fluid circuits which must be tuned to the operation of the power converter. This bearing system is costly to fabricate, difficult to tune, and high losses are incurred from the requirement for high pressures to feed the bearings.

In an attempt to reduce the complexity and losses associated with the hydrostatic bearings, MTI has tested hydrodynamic bearings implemented by inducing rotation of the piston. While reducing the losses associated with the hydrostatic design, the rotating system introduces other potential problems. These problems include the method of achieving rotation and the instability, or whirl phenomenon, that can exist in hydrodynamic bearings.

3.2.2 Bearings Results

In the following discussion, all references will refer to the piston even though the concepts apply equally well to the displacer. Possible methods to simplify the hydrostatic bearing configuration were investigated. The mechanism considered was using the translational motion of the piston to generate a hydrodynamic bearing. The idea was to introduce other possible means of piston support such that the hydrostatic requirements may be reduced and its design simplified.

3.2.3 Alternative Bearing Concept

The hydrodynamic geometry considered was the Rayleigh step pad. Although there are other load-generating configurations in addition to the Rayleigh step pad, study was limited to this geometry as a representative case. Due to the reciprocating motion of the piston, any hydrodynamic bearing configuration must generate lift in both directions. This can only occur with a symmetric (to both directions) lifting surface when non-linearities are present. At high bearing numbers, the gas compressibility is one such non-linear mechanism. Unfortunately, the piston speeds attained in this application are more likely to be in the linear incompressible flow regime, with little compressibility influence. Another non-linear mechanism is the tendency for flow to separate at abrupt changes in flow area. This effect is different for flows approaching a forward- or backward-facing step, and therefore, the combination of a forward-facing and a backward-facing Rayleigh step pad may generate net lift in both directions. Figure 3 shows a possible location for the step pads.

In addition to the hydrodynamic support possible with the Rayleigh step pads, hydrostatic support may be generated with the use of a lifting geometry at the ends of the piston, as shown in Figure 4. As the piston displaces to one end of its stroke, the leakage flow may be routed through step pads to help center the piston radially on the high-pressure end. As shown in the figure, the high-pressure working fluid may also be routed directly to a hydrostatic port on the opposite end of the piston to assist in supporting the piston on the low pressure end. Note that a step pad is shown only for illustration purposes. Since this is a pressure-driven flow (Poiseuille) rather than a slider-driven flow (Couette), the step pad geometry required to achieve lift may be different.

This configuration shown in Figure 4 has the potential to support the piston at both ends of its stroke when the piston velocity is zero. At the point of maximum velocity at the center of its stroke, the piston can generate centering hydrodynamic lift through the use of centrally located step pads as shown in Figures 3 and 4.

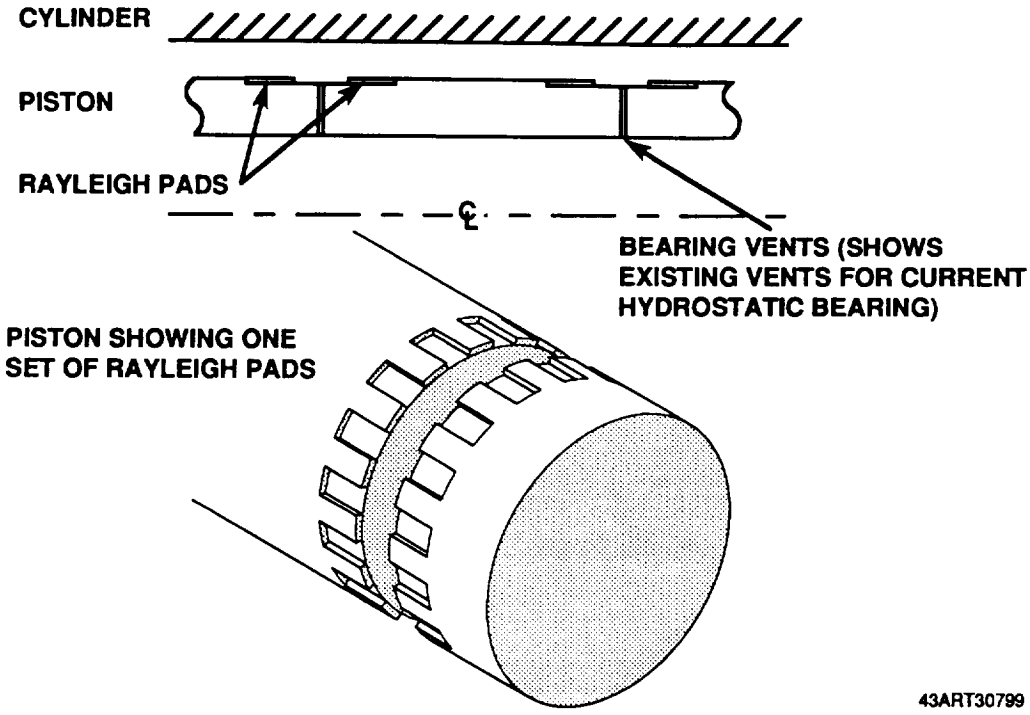

Figure 3. Rayleigh Step Pad Hydrodynamic Bearing Concept

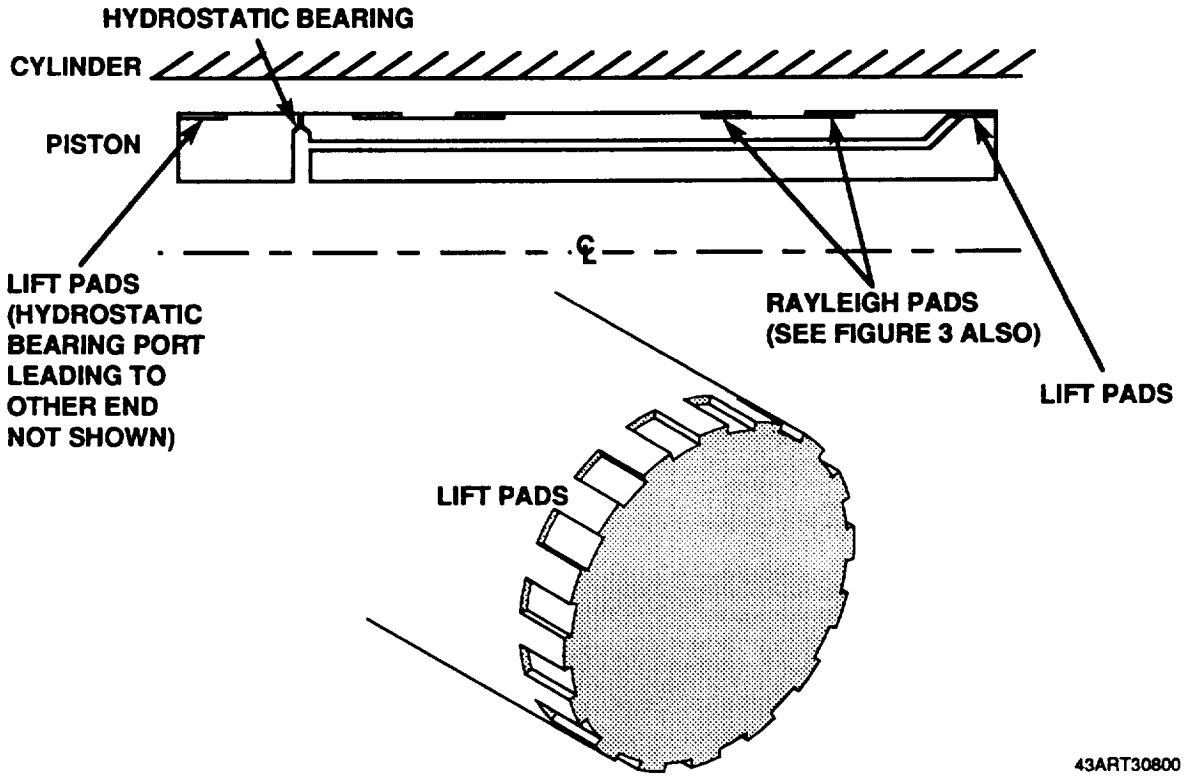

Figure 4. Lift Pad End Support Concept

The proof of concept lies in the evaluation of net lift generated by a pair of Rayleigh pads facing in opposite directions. This could be accomplished by existing computational fluid dynamics (CFD) codes. Since this is a classic fluid dynamics problem, it is possible that these solutions already exist for similar geometries and the above evaluation could be accomplished easily.

As previously mentioned, these concepts may not alleviate the necessity for a basic hydrostatic bearing system. They may, however, generate sufficient influence to allow a reduction in requirements for the hydrostatic bearing design. This could lead to lower fabrication costs, fewer bearing tuning difficulties, and lower bearing losses. On the other hand, analysis may show the described system may be able to completely replace the conventional hydrostatic design.

3.2.4 Bearings Conclusions/Recommendations

It is recommended that preliminary computations be performed for various alternative geometries for the bearing concepts discussed above using a computational fluid dynamics code such as FLUENT. If sufficient lift can be achieved at the piston speeds and pressures typical of this application, then further design work could be performed. The complexity of the resultant bearing system and its effect on power converter performance must then be compared to the baseline hydrostatic bearing.

3.3 Heat exchangers

3.3.1 Cooler

3.3.1.1 Cooler analysis

The Space Power Demonstrator Engine (SPDE) was the first NASA/MTI Stirling space power converter. The SPDE tube and shell cooler design was reviewed and the following areas for performance/ reliability improvements were noted: reduce the number of braze joints (each SPDE cooler has about 1600 tubes), increase the heat transfer surface area, and reduce the hydraulic diameter. The Component Test Power Converter (CTPC) is the next generation NASA/MTI power converter. Its cooler design was also reviewed and found to incorporate all of these improvements. It has fewer tubes and therefore, fewer braze joints, fins have been added within each tube to increase the heat transfer surface area, and there is a center body in each tube reducing the hydraulic diameter. The review of the CTPC cooler design included a brief examination of heat exchanger performance, and the conceptual development of an alternative cooler concept.

3.3.1.2 Cooler results

A spreadsheet model of the cooler was developed to evaluate possible improvements in heat transfer and pressure drop. The model evaluates the affect of changes in physical dimensions on surface areas and Reynold's number (which in turn affects heat transfer coefficients and friction factors). Using the current CTPC design configuration, no improvement in heat transfer was found without a substantial increase in pressure drop. The spreadsheet model did indicate a small reduction in pressure drop with the same heat transfer would be possible by using fewer, wider slots in the tube inserts. A GLIMPS simulation run also indicated a slight decrease in pressure drop, but no improvement in overall converter power or efficiency. The results are shown in Table 1. Assuming equivalent converter performance, the cooler configuration with fewer, wider slots may be desired since this would be slightly less expensive to manufacture.

Table 1. Cooler Analysis Results

	CTPC Design GLIMPS Model	"Improved" Design Spreadsheet Model	"Improved" Design GLIMPS Model
Heat transfer (W)	-3.87E4	-3.87E4	-3.87E4
Press drop (N/m^2)	2.11E4	1.73E4	1.99E4
Gross Power (W)	1.73E4	-	1.73E4
Gross efficiency (percent)	0.302	-	0.302

3.3.1.3 Alternative cooler concept

A new cooler configuration using large concentric tubes with alternating gas and coolant tubes (see Figure 5) was examined. Flow cross section areas and heat transfer surface areas compared as shown in Table 2.

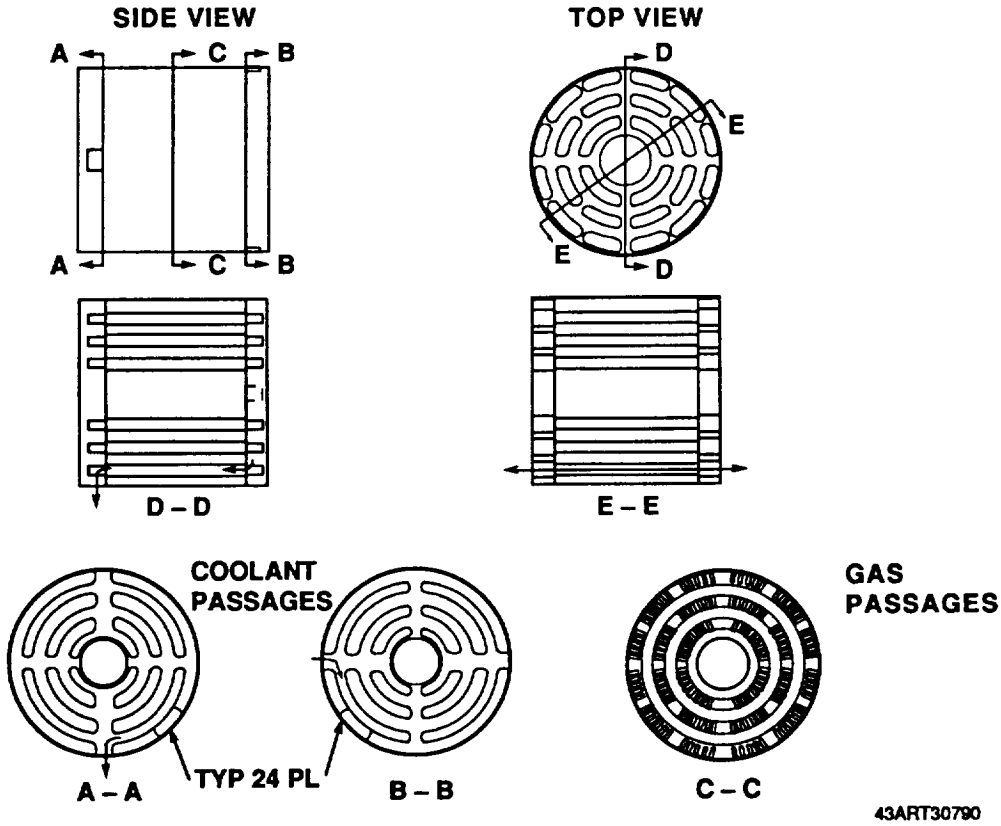

Figure 5. Concentric Tube Cooler Concept

Table 2. Alternative Cooler Concept Comparison

	Gas Flow Cross-Section Area, cm^2 (in^2)	NaK Flow Cross-Section Area, cm^2 (in^2)	Liquid Side Heat Transfer Surface Area, cm^2 (in^2)
CTPC design	20.0 (3.10)	126 (19.6)	3850 (597)
New concept	19.7 (3.05)	115 (17.8)	4170 (647)

The concentric tube concept would provide similar gas flow and NaK flow cross sectional areas, but provide a higher surface area for heat transfer. However, this concept has many unresolved issues (fabrication and assembly difficulties, and stress questions) that would have to be addressed before it could be properly evaluated.

3.3.1.4 Cooler conclusions/recommendations

The current CTPC cooler design is a significant improvement compared to the SPDE design. It is recommended that a detailed thermal/pressure drop analysis of the use of fewer, wider gas passages in the cooler inserts be conducted; fewer slots would reduce fabrication costs. A detailed analysis of the concentric tube cooler design should be undertaken to determine if any performance improvement is possible.

3.3.2 Heater

3.3.2.1 Heater analysis

The CTPC starfish heater consists of radial fins around a central hub with multiple gas passages in each fin. The outside of the fins serves as the condenser for the sodium heat pipe. The CTPC starfish heater design was compared to the SPDE shell and tube design (with about 1600 tubes per cylinder) and the following improvements were noted: the newer design is heat pipe compatible, and the monolithic design eliminates welding/brazing gas passage tubes and probably increases strength.

While the monolithic design offers advantages, it also leads to some fabrication concerns. The first is the need to plunge EDM the fins with relatively tight tolerances. Similarly, STEM (shaped tube electrolytic machining) drilling the high length-to-diameter ratio holes in the fins, with thin walls, will require some careful process development.

3.3.2.2 Heater results

A spreadsheet model of the heater was developed. Using the current CTPC design configuration, no improvement in heat transfer was found. However, a reduction in pressure drop with the same heat transfer was possible with an increased hole width and a reduced height. There was also a lower overall number of holes which may reduce manufacturing cost. A GLIMPS simulation run verified the trend in pressure drop, but did not predict any improvements in overall converter power and efficiency. See Table 3.

Table 3. Heater Analysis Results

	CTPC Design GLIMPS Model	"Improved" Design Spreadsheet Model	"Improved" Design GLIMPS Model
Heat transfer(W)	5.74E4	5.79E4	5.73E4
Pressure drop(N/m^2)	2.01E4	1.41E4	1.57E4
Gross Power (W)	1.73E4	-	1.73E4
Gross efficiency (percent)	0.302	-	0.301

3.3.2.3 Alternative Heater Head Concepts

Several alternative methods of fabricating the starfish heater head were investigated to alleviate the possible fabrication difficulties of the monolithic structure, especially the forming of the working fluid passages.

The first alternative heater head concept developed was the pressed fin concept. In this concept, individual two piece fins would be fabricated. Gas passages would be machined into plate stock using normal milling or EDM practices, the recast layer removed, and then the plate would be TLPD bonded to a second piece of plate (see Figure 6) forming the fin. The fins could then be final machined.

Next, the fins would be assembled into slots in the top and bottom plates of the hub. The slots would be machined to create an interference fit with the fins to provide the proper load for TLPDB the fins to the hub. Assembly of the fins into the hub would be accomplished using a shrink fit. Finally, the fins would be bonded to the hub with the appropriate TLPDB temperature cycle.

The pressed fin design would have the major advantage of easy fabrication of the holes in the fins compared to the current heater head design, and would also allow for leak testing of the individual fins before completion of the heater head.

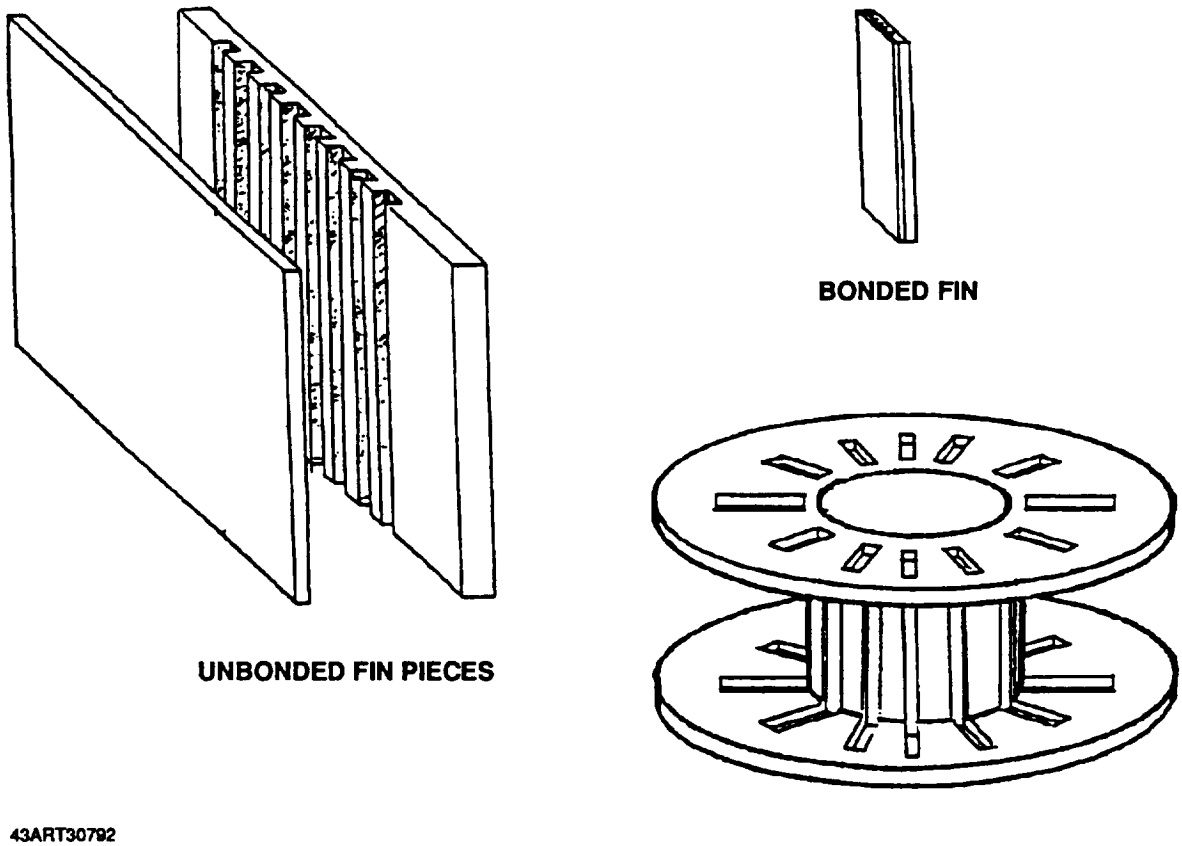

Figure 6. Pressed Fin Heater Head Concept

However, there would be disadvantages to the pressed fin design as well. The interference fit assembly of the fins into the slots in the heater head would be difficult. Of even greater concern is the relatively high number of features that would require tight tolerances. Fifty fins and 100 slots would have to be machined to provide the proper interference fit. This is feasible, but would be difficult and expensive.

The next alternative fabrication concept examined was a laminated heater head design. In this approach, the gas passage portion of the heater head would be made up of relatively thin laminates TLPD bonded together (see Figure 7). Each laminate would be electrochemical machined (ECM). The laminates would then be stacked together and bonded.

The laminated design would eliminate the assembly concerns associated with the pressed fin design. The artwork would include tooling holes, and the laminates would be stacked on alignment pins prior to bonding, making assembly straight-forward. In addition, alignment of the holes between laminates would be established by the ECM artwork.

However, there are potential problems with the laminated heater head concept. It would require a high number of laminates (100 to 200) with tight tolerances, particularly on surface finish and parallelism. If several laminates with thin sections in the same part of the laminate where stacked together, a low strength bond could result. Also, tolerance stack-ups between the laminates and tooling could lead to hole misalignment. Similarly, variation in hole diameter would lead to a poor surface finish on the inside of the holes. Finally, Udimet 720 sheet stock is not currently available. None of these problems would make the design unworkable, but would require a fairly significant development effort to overcome.

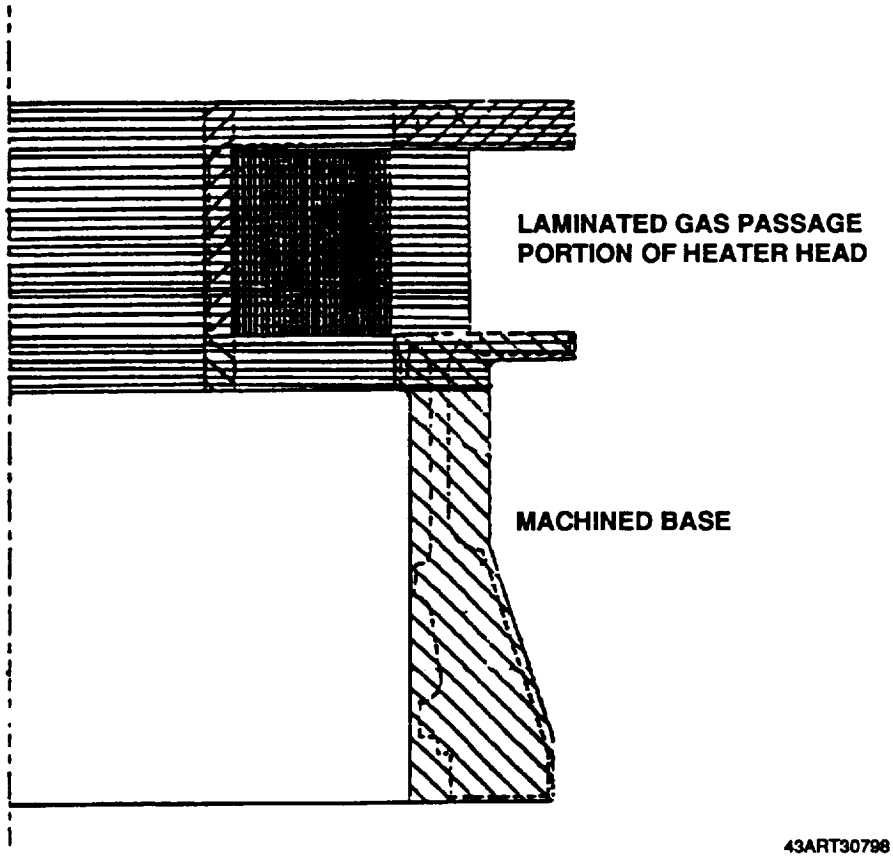

Figure 7. Laminated Heater Head Concept

The third alternative heater head concept examined was the sandwiched fin design. This design would also be fabricated using the TLPDB technique. The process features separate heat exchanger fins. Each fin would be made from two pieces similar to the pressed fin concept (see Figure 8). The gas passages would be wire EDMed into one of the two pieces, the recast layer removed, and then the two pieces would be TLPD bonded together. Not only would this approach greatly simplify the machining of the gas passages, but would also allow for leak testing of the individual fins before completion of the heater head.

The sandwiched fin design differs from the pressed fin design in the way the fins are aligned and bonded to the heater head. The sandwiched fin heater head is a three piece design, consisting of 50 separate fins, the top plate/hub, and the base (see Figure 9). Slots would be EDMed into the top plate and base to allow the gas to pass into the fins. After fabrication and leak testing, the fins would then be placed between the base and top plate. Alignment pins would be placed through the slots into the second and last gas passages in each fin to ensure alignment.

The three sections of the heater head would then be joined using TLPDB. The configuration of the heater head after TLPDB is shown in Figure 10. A leak test of the bonded assembly could be performed. Process control and test coupons, in conjunction with the leak testing, could be used to ensure bond integrity.

3.3.2.4 Heater conclusions

Compared to the SPDE heater, the CTPC starfish design has significantly reduced the number of joints required and adds heat pipe compatibility. It is recommended that a detailed thermal/ pressure drop analysis of the use of fewer, wider gas passages in the heater fins be conducted. The sandwiched fin fabrication process using TLPDB is recommended as an alternative heater head fabrication method. Although this approach would introduce more joints to the design, TLPDB has been very reliable and repeatable in production applications, and would alleviate concerns about ED machining the fins and STEM drilling the holes.

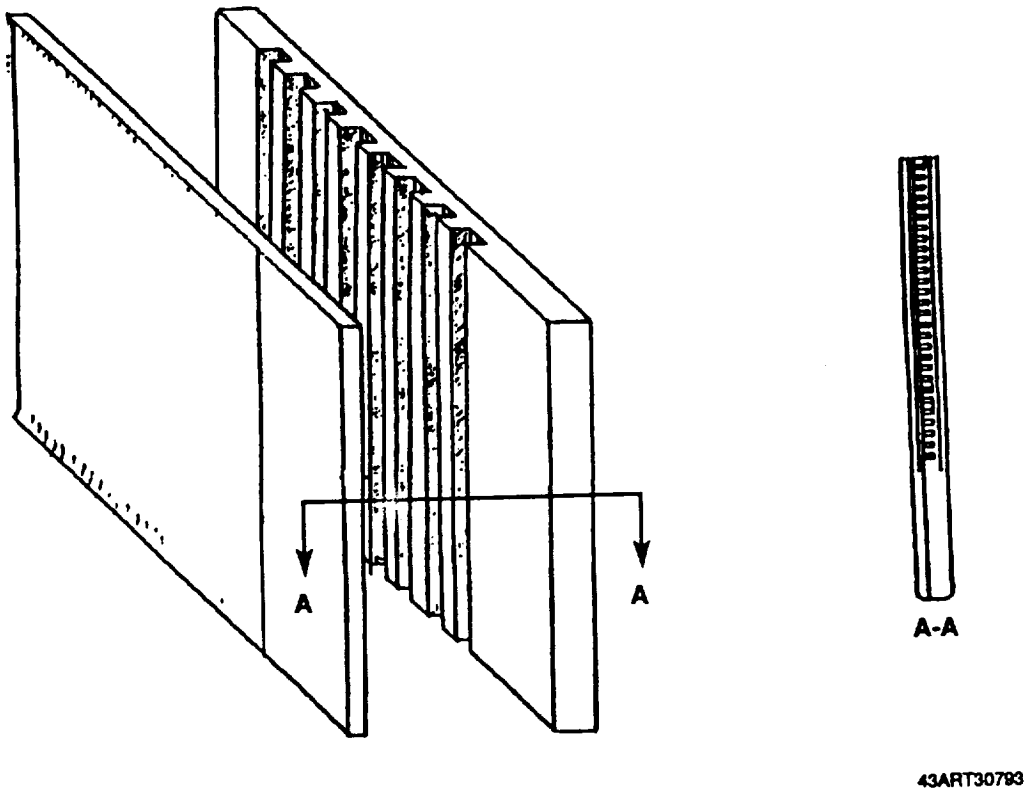

Figure 8. Two-Piece Fin Construction

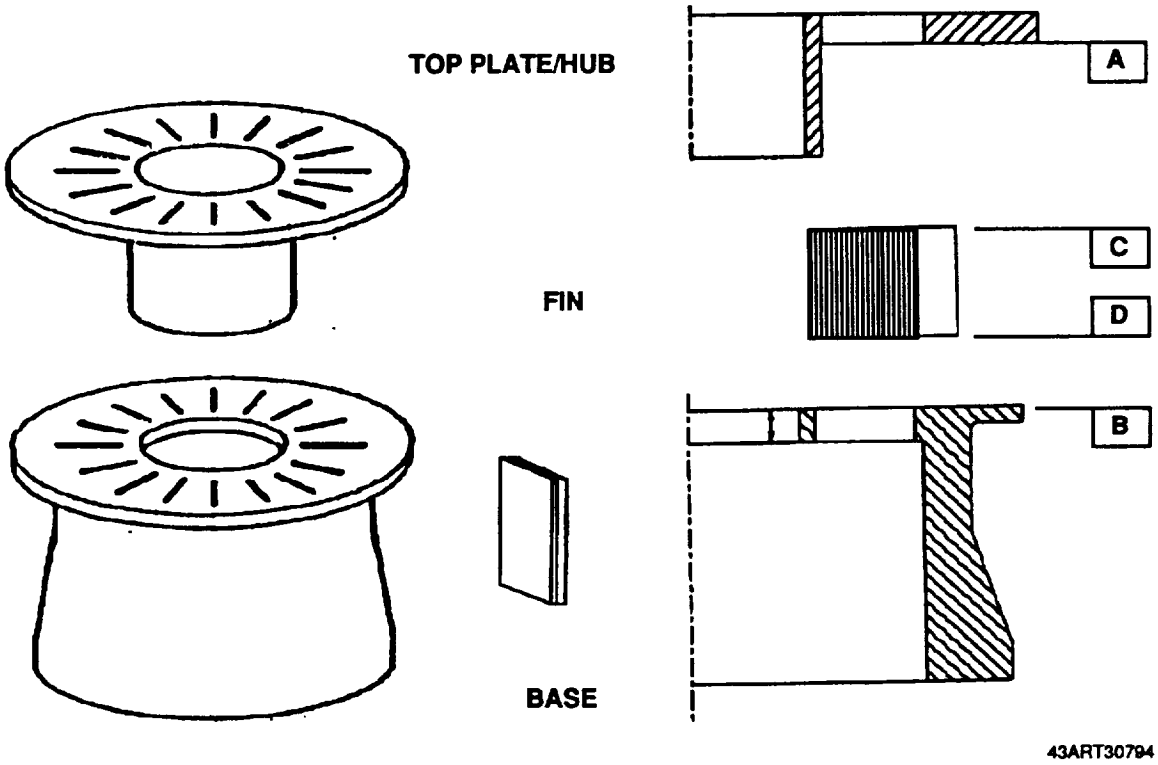

Figure 9. Sandwiched Fin Heater Head Subassemblies

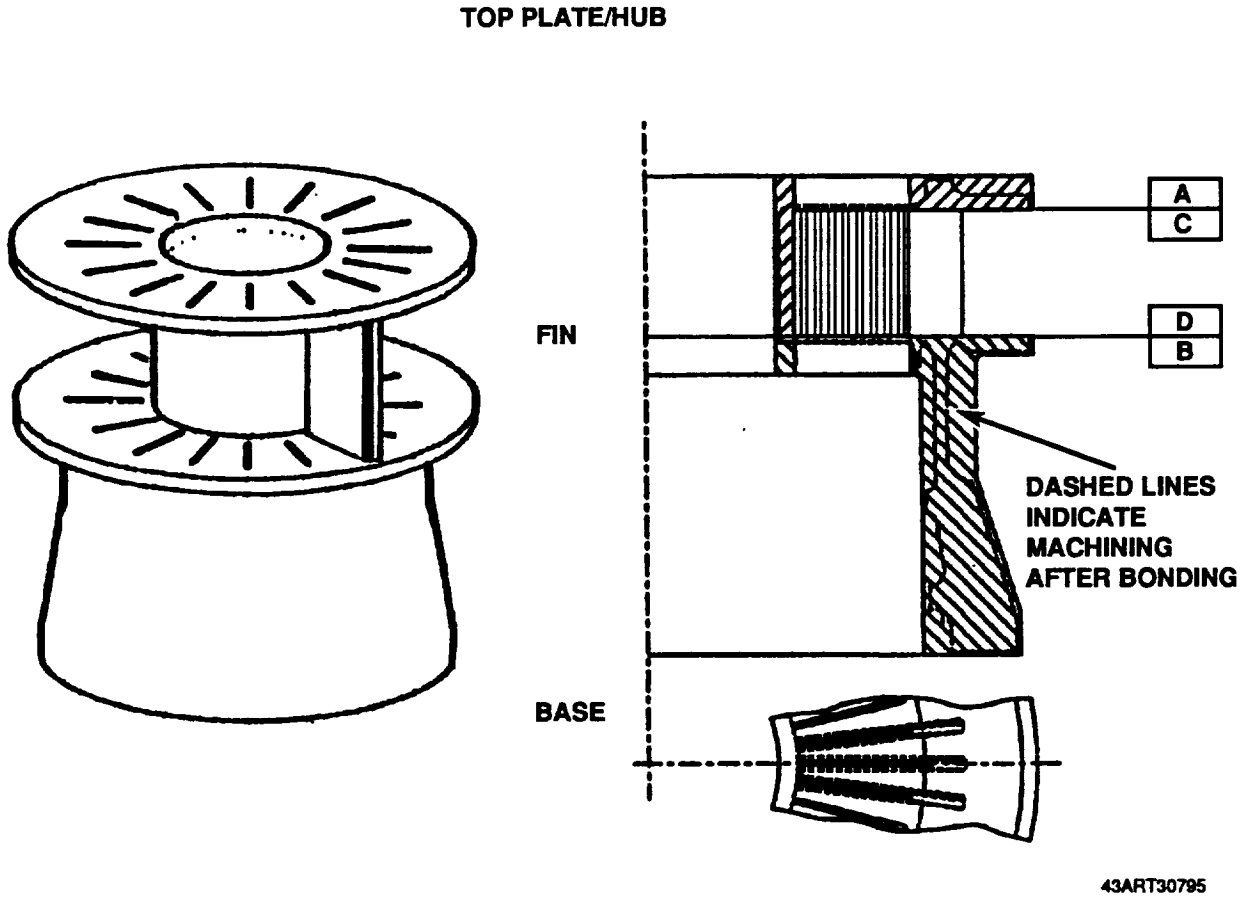

Figure 10. Sandwiched Fin Heater Head Bonded Assembly

4. SUPPORTING ANALYSIS

4.1 Power Converter Performance Analysis

4.1.1 GLIMPS Simulation

The power converter analysis was performed using the GLIMPS computer software from Gedeon Associates.

Before the power converter simulation could begin, the preferred version of GLIMPS had to be selected. NASA Lewis' experience with GLIMPS 2.1 indicated that cylinder heat transfer may be underestimated and therefore, high cylinder heat transfer multipliers (H-multipliers) had to be used to match actual power converter test results. GLIMPS 3.02 includes revised calculations of cylinder heat transfer; however, these have not been validated and may overestimate cylinder heat transfer. It was finally decided to use GLIMPS 3.02 with H-multipliers of 0.25 in the compression and expansion spaces; these factors gave close agreement with SPDE test results. This decision was based largely on the fact that GLIMPS 3.02 calculates both piston P-V power and indicated power.

NASA Lewis gave recommendations on the iteration tolerance and the number of cells to use in the cooler, regenerator, and heater in the GLIMPS simulation. In addition, NASA Lewis provided a sample GLIMPS post-processor and assistance in determining post-processor input variables. The post-processor calculates power converter losses not included in the basic GLIMPS simulation.

The performance analysis was done for the CTPC design based on its similarity to the reference Udimet 720 power converter and the availability of information for modeling.

Input data for the GLIMPS simulation came from several sources. Information provided by NASA Lewis and MTI in the program kick-off meeting included operating temperatures, frequency, and stroke. NASA Lewis provided additional information on operating clearances, and data to determine the cylinder H-multipliers. Finally, most of the physical dimensions were estimated from the MTI layout drawing of the power converter. Some difficulty was experienced in accurately determining dimensions from the two-dimensional layout drawing.

4.1.2 GLIMPS Results

A summary of the GLIMPS results for the CTPC is given in Table 4. Plots of key power converter temperatures and pressures are given in Appendix 1 as Figures 15 through 18.

Table 4. GLIMPS Simulation Results Summary

Power output (kW):	15.7 indicated 15.5 piston P-V
Efficiency (percent):	26.4 indicated 26.2 piston P-V
Temperatures (K) (mean, oscillation amplitude)	
Compression space:	gas: 525.5, 24.1 wall: 526.4, 0.9
Regenerator mid-point:	gas: 771.4, 4.0 wall: 771.3, 2.3
Expansion space:	gas: 1015, 44.6 wall: 1017, 1.3
Pressures (N/m^2)	
Expansion space:	1.500E+7, 1.667E+6

The GLIMPS simulation results were used as inputs to the materials studies. No internal power converter modifications were required to use the TLPDB technique, so no analysis of the effects of power converter modifications was required.

4.1.3 GLIMPS Conclusions

The CTPC simulations indicated that GLIMPS is very sensitive to input parameters. Therefore, accuracy in the input data is extremely important.

Another concern associated with using the GLIMPS software is the understanding of cylinder heat transfer. GLIMPS 3.02 revised calculations predict much larger values of cylinder heat transfer than does GLIMPS 2.1; these revised calculations have not been validated. H-multipliers on the cylinder heat transfer can be used to match analysis predictions to test data. However, other losses may also not be properly quantified. A description of the NASA Lewis program to better understand the losses in a Stirling converter is given in reference 2.

4.2 System Optimization

4.2.1 System Optimization Analysis

For the system-level optimization analysis, the system configuration was defined with input from NASA Lewis. The configuration was as follows:

- Multiple power converters with one spare
- One reactor with shielding
- An intermediate liquid-metal loop between the reactor liquid-metal loop and the Stirling power converters
- One radiator for each power converter

The mass algorithms used in the system optimization model came from several sources. The power converter mass was obtained from algorithms based on the MTI scaling study (reference 3). The reactor and shielding algorithms came from published papers on the SP-100 space reactor. The shielding algorithm was modified to account for the higher allowable dose rates recommended by NASA Lewis. The radiator mass was calculated based on a 5 kg/m2 specific mass. Other mass algorithms were empirical relationships based on GFSD experience, scaled from known or calculated masses. Data points for the intermediate liquid-metal loop and controls masses, for example, were obtained from a NASA paper presented at the 1991 Nuclear Space Power Symposium. For GFSD, this was the initial formulation of a Stirling systems analysis code and the results should be considered as an early estimate for flight systems.

The optimization routine used in the model was the same routine used by GFSD on Brayton system optimizations. The routine sequentially calculates partial derivatives of the optimization parameter with respect to the independent variables, and resets the variable values if there is improvement. This continues until no further improvement in the optimization parameter is possible.

4.2.2 System Optimization Results

Optimizations were run at two gross electrical power output levels: 100 and 500 kW_e. The results are shown in Tables 5 and 6.

Table 5. 100-kW_e System Optimization Results

100-kW_e case Configuration: Hot end temperature = 1050 K Four operating units, one standby unit (dual opposed units)	
Optimization results: Temperature ratio Stirling power converter specific mass Stirling cycle efficiency Radiator area System mass	 1.90 4.95 kg/kW_e 25.8 percent 108 m^2 = 1.1 m^2/kW_e 3387 kg = 33.9 kg/kW_e
System mass breakdown: Stirling power converters Reactor + primary cooling Shield Radiators Intermediate HSHX Power conditioning Structure Total	 619 kg 864 kg 168 kg 542 kg 582 kg 304 kg 308 kg 3387 kg

Table 6. 550-kW_e System Optimization Results

550-kW_e case Configuration: Hot end temperature = 1050 K Five operating units, one standby unit (dual opposed units)	
Optimization results: Temperature ratio Stirling power converter specific mass Stirling cycle efficiency Radiator area System mass	 1.90 5.25 kg/kW_e 27.6 percent 544 m^2 = 1.0 m^2 kW_e 11754 kg = 21.4 kg/kW_e
System mass breakdown: Stirling power converters Reactor + primary cooling Shield Radiators Intermediate HSHX Power conditioning Structure Total	3465 kg 1914 kg 399 kg 2719 kg 1359 kg 830 kg 1068 kg 11754 kg

It may be noted that at both power levels, the system optimized at a temperature ratio of 1.9. The temperature ratio is the Stirling converter hot-end temperature divided by the converter cold-end temperature.

In addition to the optimization study, a sensitivity analysis was performed. Converter specific mass (SM) and temperature ratio (TR) were each varied from the baseline optimum. The results are given in Tables 7 and 8.

Table 7. 100-kW_e System Sensitivity Analysis Results

100-kW_e Case	SM (kg/kW)	TR	System Mass (kg)	System Mass Delta (percent)
Baseline	4.95	1.9	3387	-
	4.95	1.7	3432	+1.3
	4.95	2.1	3449	+1.8
	4.95	2.3	3612	+6.6
	4.95	2.5	3902	+15.2
	4.95	2.7	4393	+29.7
	4.95	2.9	5272	+55.7
	4.0	1.9	3419	+0.1
	4.5	1.9	3394	+0.0
	5.5	1.9	3395	+0.0
	6.0	1.9	3414	+0.1
	6.5	1.9	3444	+1.7
	7.0	1.9	3482	+2.8
	7.5	1.9	3529	+4.2
	8.0	1.9	3582	+5.6

Table 8. 550-kW_e System Sensitivity Analysis Results

550-kW_e Case	SM (kg/kW)	TR	System Mass (kg)	System Mass Delta (percent)
Baseline	5.25	1.9	11754	-
	5.25	1.7	12058	+2.6
	5.25	2.1	11985	+2.0
	5.25	2.3	12698	+8.0
	5.25	2.5	14029	+19.4
	5.25	2.7	16370	+39.3
	5.25	2.9	20723	+76.6
	4.0	1.9	12229	+4.0
	4.5	1.9	11909	+1.3
	5.0	1.9	11771	+0.1
	5.5	1.9	11765	+0.1
	6.0	1.9	11859	+0.1
	6.5	1.9	12035	+2.4
	7.0	1.9	12280	+4.5
	7.5	1.9	12586	+7.1
	8.0	1.9	12950	+10.2

It may be noted that the Stirling power conversion systems have a much higher mass sensitivity to variations in temperature ratio than to variation in power converter specific mass. This is to be expected because temperature ratio has a large effect on conversion efficiency (which affects reactor, shielding, heat exchanger, and radiator masses) and radiating temperature (which also affects radiator mass). Power converter specific mass affects a smaller portion of the overall system.

4.2.3 System Optimization Conclusions

At power levels of 100 kW_e and 550 kW_e, with the configuration defined with inputs from NASA Lewis, the system optimized at a temperature ratio of 1.9. The Stirling power conversion systems have a much higher mass sensitivity to variations in temperature ratio than to variation in power converter specific mass.

5. MATERIALS STUDIES

As Stirling power converter technology has evolved in recent years, a trend toward high-pressure, high-temperature power converters has pushed the limits of standard nickel-base alloys. These alloys, such as Inconel 718, have established joining methods with predictable mechanical properties.

When one considers those alloys that can meet high-pressure, high-temperature, and long-life requirements, such as Udimet 720, the question of joining methods may limit the use of these alloys in the manufacture of Stirling power converters. Udimet 720 has been selected by NASA/MTI as the heater head material for the long-life Stirling space power converter.

Work conducted in the turbine engine industry has shown that a joining process called transient liquid-phase diffusion-bonding (TLPDB) can be successfully applied to the newer, high-temperature nickel-base alloys that are difficult to fusion weld. This process may be useful in solving joining problems with regard to Stirling power converters and the use of the Udimet 720 alloy. In addition, the Stirling power converter uses liquid metals for heat transfer that may pose a structural materials compatibility problem with particular interest in corrosion, mass transfer, and embrittlement mechanisms.

The goals of the materials studies were the identification of feasible joining methods that might be used on Udimet 720, the theoretical development of a transient liquid phase diffusion bonding method which may be applied to specific Stirling power converter designs, and consideration of materials compatibility issues with regard to liquid metals.

The materials studies task was conducted in three sections:

- Alternative joining techniques,
- TLPDB study,
- Liquid metals compatibility.

5.1 Alternative Joining Techniques

This task was defined as an effort to review an existing design including material selections and stress levels with regard to alternative joining methods.

5.1.1 Alternative Joining Techniques Analysis

The analysis of alternative joining techniques and the assembly sequence were conducted in concert to ensure compatibility of the bonding methods and assembly process. As discussed in 3.1.1 above, the following approach was used:

1. Identify materials for each joint
2. Identify stress levels for each joint
3. Identify materials joining options
4. Establish preliminary assembly process steps
5. Determine if the joining option at each process step
   a) Is compatible with materials and sub-assemblies from previous steps
   b) Meets the joint design drivers and requirements
6. Modify process steps and/or joining options based on results of step 5
7. Establish recommended assembly process steps

The joints examined are shown in Figure 1. Table 9 gives a description of each joint and the materials and strength requirements defined by MTI. In addition to the requirements shown in Table 9, very low joint deformation is allowed for proper power converter performance, and very high joint integrity is required for space applications.

A review of the literature and aerospace industrial joining practices was conducted to identify possible methods consistent with nickel-base superalloys. These processes include:

- Tungsten inert gas (TIG) welding
- Brazing
- Diffusion bonding (DB)
- Laser welding (LW)

- Friction welding (FW)
- Transient liquid-phase diffusion-bonding (TLPDB)
- Electron beam (EB) welding

Table 9. Joint Requirements

Joint Number	Description	Materials	Grain Size (ASTM No.)	Maximum Temperature (K)	Critical Stresses (psi x 1000)
2	Joins two halves of dual opposed converter	U720/U720	00-2/00-2	1050	85 ±73
3	Heater head transition joint between U720 and IN718	U720/IN718	00-2/4-6	811	296 ±33
4	Regenerator outer wall to heater head	U720/U720	8-10/8-10	1050	159 ±27
6	Cooler body to heater head	IN718/IN718	4-6/4-6	525	345 ±41
7	Heat pipe flange to heater head	IN718/U720	3-4/00-2	1050	21 ±21
	Heat pipe to heat pipe flange	IN718/IN718	3-4/3-4	1050	21 ±21

Each process has a different set of physical limitations and resultant joint qualities. Those items were identified and are presented in Table 10 (reference 4).

Table 10. Process Comparison

Process Limitation	Process Requirement						
	TLPDB	EB	TIG	Braze	DB	FW	LW
Close tolerance pre-machine	yes	yes	no	no	yes	no	yes
Post machining	no	yes	yes	no	yes	yes	yes
Special cleaning	yes	no	no	yes	yes	no	no
Coating	yes	no	no	yes	no	no	no
Special tooling	yes	yes	no	yes	yes	yes	yes
Line of sight required	no	yes	yes	no	no	no	yes
Geometric constraints	yes	no	no	no	yes	yes	no
Vacuum chamber required	yes	yes	no	yes	yes	no	no
Deformation required	no	no	yes	no	yes	yes	no
High porosity joint	no	no	yes	yes	no	no	no
Poor room-temperature properties	no	no	no	yes	no	no	no
Poor high-temperature properties	no	no	no	yes	no	no	no
Post heat treat required	yes	yes	yes	no	yes	yes	yes
Thermal cycle required	yes	no	no	yes	yes	no	no
Strain age cracking	no	yes	yes	no	no	no	yes
Grain growth	yes	no	no	no	yes	no	no

Examination of the requirements of the joints shows a very high quality process is needed for each joint to meet the high joint integrity requirement and the high temperature mechanical properties, near those of the parent material. A review of Table 10 shows that brazing and TIG joining techniques very often result in porosity, and brazing does not normally yield high mechanical properties.

The literature search revealed that nickel-base superalloys containing aluminum and titanium with combined concentrations in excess of approximately 4 percent are subject to strain age cracking from fusion-welding processes without special welding pre- and post-weld conditioning (reference 5) (see Figure 11). The strain age cracking condition is caused by the aluminum and titanium forming brittle phases during solidification which does not allow the alloy to distribute stresses from weld contraction strains during post-weld heat treatment. Weld cracks normally occur with time or during the thermal ramp of post-weld heat treat (reference 5). Processes such as TLPDB, brazing, DB, and FW are not limited in this regard since the parent metal is not melted. Udimet 720 would therefore not be easily fusion welded without cracking problems due to the high aluminum and titanium concentrations. Joints 2, 3, 4, and 7 all use Udimet 720 which suggests EB, TIG, and LW may be difficult to use without strain age cracking.

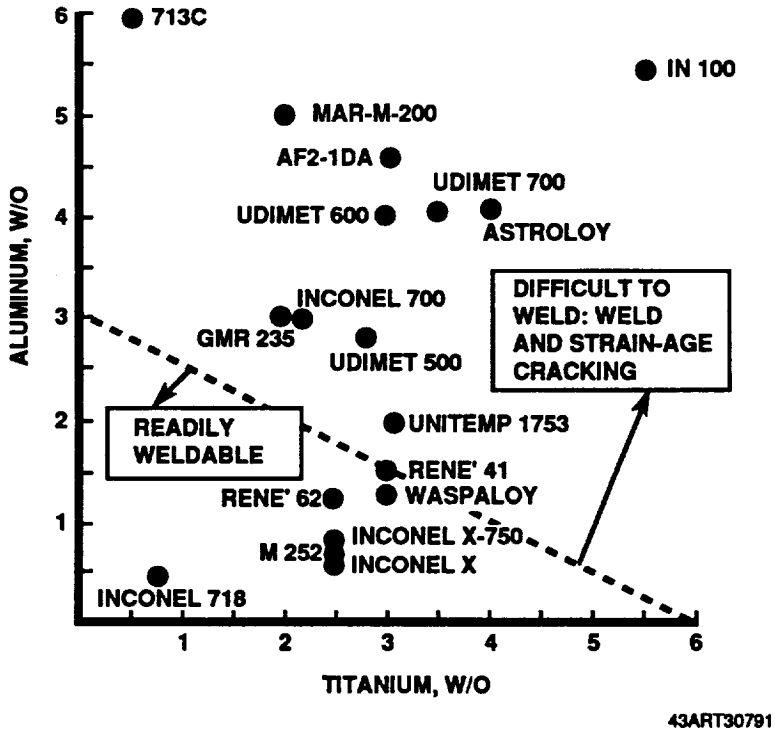

Figure 11. Difficult-to-Weld and Readily Weldable Gamma Prime Strengthened Alloys

Reference 6 describes a study on the mechanical behavior of a nickel-base superalloy welded with EB and FW. Tests were conducted showing no difference in strength in tension at room temperature and 700 K (800°F), low cycle fatigue, 1 percent creep, and stress rupture between the joining techniques. The FW process has also been used with success on nickel-base superalloys that are sensitive to strain age cracking. However, both FW and solid-state diffusion-bonding require extensive distortion of the parent materials (reference 4). Since all of the joints require very low deformation, solid-state diffusion bonding and FW were not further considered.

Examination of joint 6, as shown in Figure 1, shows no line of sight without a design change affecting the use of EB, TIG, or LW for this joint. It is understood that modifications have been made by MTI to provide this line of sight for the reference long-life power converter.

The TLPDB process does result in grain growth that may limit its consideration for joints 3, 4, 6, and 7. The use of TLPDB will depend on the availability of Inconel 718 and Udimet 720 with small enough initial grain sizes, such that after grain growth during TLPDB processing, the final grain size requirements of Table 9 are met. In the case of Inconel 718, initial grain sizes as small as ASTM 10 have been achieved using a forging process (reference 7), which would make TLPDB a possibility. In the case of Udimet 720, material inspected at GFSD has shown initial grain sizes as small as ASTM 12 (with an unknown processing history). This data suggests that TLPDB can be considered for the Stirling power converter application.

5.1.2 Alternative joining techniques results

A list of possible joining techniques based on the discussion presented above is contained in Table 11. This table is based on line of sight, strain age cracking, strength, deformation, and joint defect requirements compared with joining processing limitations.

Table 11. Possible Joining Techniques for Each Joint

Joint	Recommended Process
2	TLPDB, EB*
3	TLPDB, EB*
4	TLPDB, EB*
6	EB**, TLPDB
7	TLPDB, EB*
	EB, TIG

* May require extensive process development due to strain age cracking problems

** Line of sight required

Inspection methods that can be used for TLPDB include the following:

- Ultrasonic inspection - used on thin parts
- Pressure test - used in pressure vessel applications
- Mechanical test - used in applications designed to withstand external loads
- Microstructure test - requires special geometrical configuration
- Microstructure test coupon - sacrificial test piece run with actual parts

TLPD bonds are normally not repairable if they are found to be defective. However, most alloy systems, including the Udimet 720 application under consideration, can be seal repaired using a powder-brazing paste of a similar composition to the original bond aid. This repair does require an additional thermal cycle, but the duration at temperature is normally not longer than 20 minutes.

5.1.3 Alternative Joining Techniques Conclusions

The results of the study showed that TLPDB has the lowest risk for the Udimet 720 joints, with electron beam (EB) welding being a higher-risk alternative.

5.2 TLPDB Analysis

5.2.1 TLPDB Analysis

TLPDB is a metallurgical joining process which is similar to a solid-state diffusion bond except a liquid interface (bonding aid) is used to achieve mutual contact of the bond surfaces as opposed to bond line distortion. This process is capable of achieving 95 percent joint efficiencies (joint strength as a percentage of parent material ultimate strength), without distortion or melting of the parent materials to be joined (reference 8). Line of sight is not required, but bond surfaces must have a fit conformance within the liquid thickness used to achieve mutual contact. Dissimilar metals can also be joined in most cases with the use of a proper bonding aid material.

TLPDB requires a thermal cycle which must be consistent with metallurgical thermal constraints of the alloy to be joined and allows for melting of the bonding aid and diffusion of the interface elements to form a homogenous joint with the parent material. The bond aid material is normally an alloy which has a melting point depressant, usually a eutectic that will solidify during the thermal cycle due to dilution of the depressing element. This step is called isothermal solidification as shown in Figure 12 (reference 8).

The most critical part of the design of a TLPDB process for any joining application is the selection of the bond aid material. The bond aid material's melting character must be consistent with the parent alloy heat treat constraints, and elemental homogenization must be achieved by diffusion without the formation of detrimental intermetallic phases.

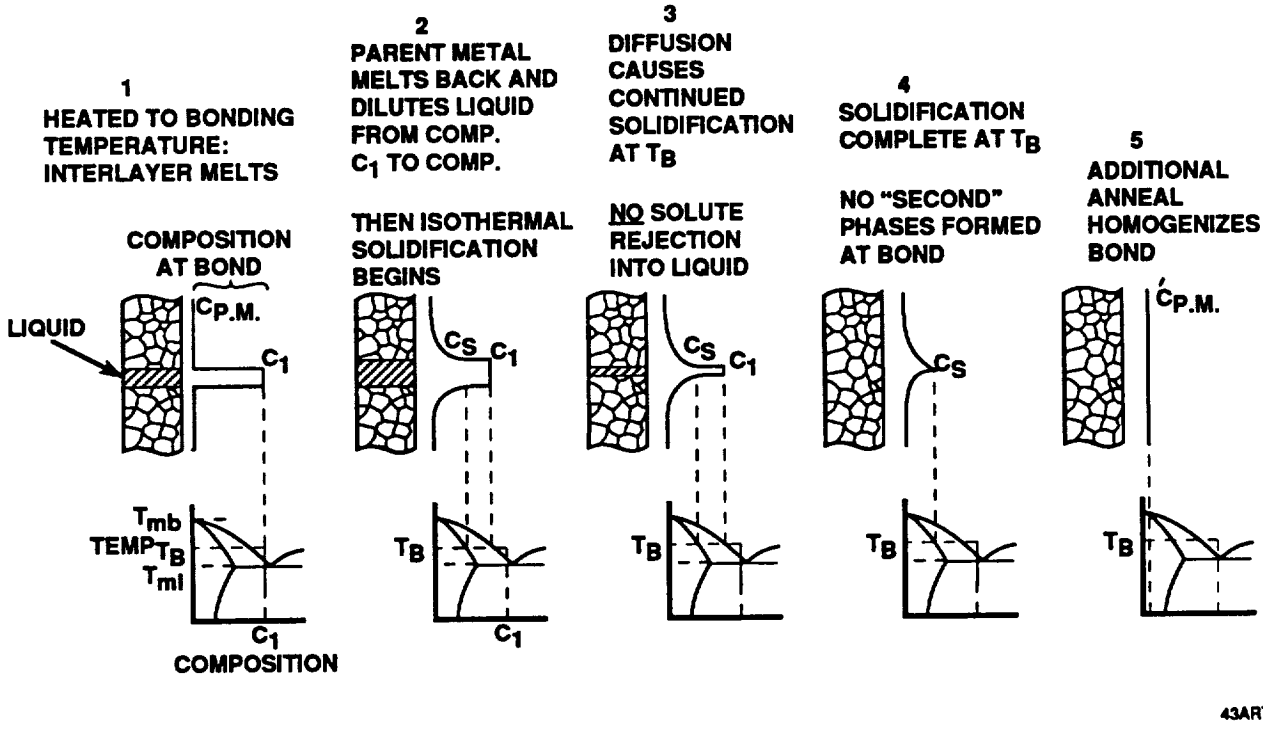

Figure 12. Mechanism of Isothermal Solidification During Transient Liquid-Phase Bonding

5.2.1.1 Phase diagram study

The first step in the TLPDB analysis was a phase diagram study. The goal of the phase diagram study was to select a binary or alloy system which would:

1) Allow a melt within the heat treatment constraints of the parent alloy,

2) Allow for isothermal solidification of the interlayer,

3) Allow for joint homogenization,

4) Minimize formation of brittle phases,

5) Have predicable properties of the alloy formed at the bond interface, and

6) Be compatible with liquid sodium

Important variables considered during the phase diagram study included:

1) The solubilities of the alloys,

2) The melting temperature,

3) The diffusion rate of primary concentrations,

4) The diffusion rate of alloying elements,

5) The solubility of alloying elements, and

6) The slope of the liquidus-solidus lines.

A table of eutectic melt temperatures, solubility, and partial diffusion rate data was generated (see Table 12). Diffusion calculations and eutectic conditions evaluations were made based on this data. The heat treat constraints of Udimet 720 require a bonding temperature between the gamma - gamma prime solvus from 720 to 1120 °C and the eutectic melt at 1250 °C.

Table 12. Binary Comparisons

Binary	Solubility Limits at 1366 K (weight percent)		Melting Temp (°C)	Diffusion Rate DT ($cm^2/s \times 10^{-11}$)	
	A:B	B:A		A:B	B:A
Al-Ni	0	8	L 660	86	
Au-Ni	M	M	E 954	1310	1.17
Be-Ni	2.7	25.5	E 1159	30810	77
Cb-Ni	8	1	L 1175		
Cu-Ni	M	M	L 1084	272	7.6
Co-Ni	M	M	L 1455	2.33	3.97
Fe-Ni	1	M	L 1425	143	3.12
Mn-Ni	92	3	E 1020		
Mo-Ni	1	36	L 1320		1.1
Pb-Ni	0	4	L 327		
Pd-Ni	M	M	E 1239		
Pt-Ni	M	M	L 1355		
Re-Ni	4	32	L 1455		
Ru-Ni	11	22	L 1455		
Si-Ni	0	8	E 967		86
Sn-Ni	0	19	L 231	0.025	
Ta-Ni	0	22	L 1362		
Ti-Ni	10	10	E 943		1.99
V-Ni	17	38	E 1205	16905	
Zn-Ni	0	32	E 419		
Zr-Ni	2	2	E 961		
B-Ni	0	0	E 1093		
P-Ni					
Hf-Ni	1	1	E 1150		

M - mutually soluble
L - lowest melting point
E - eutectic
$DT = D_o e^{-Q/RT}$
T = 1366 K = 2000 °F
R = 0.001987 Kcal/mole/K

One purpose of this table was to determine whether any element could be applied to the bond surface to lower the melt temperature of a thin layer below the eutectic melting temperature of the substrate nickel alloy. Ideally one would like to see mutual solubility to avoid formation of intermetallics and a high diffusion rate to dilute the solute as much as possible within the heat treat constraints of the substrate nickel-base alloy.

Information from Table 12 shows the mutually soluble elements with Ni are:

Au, Co, Cu, Pd, Pt, Ni

If one were to take those binaries with nickel that are mutually soluble and examine self-mating combinations, a low melt eutectic may be a possibility. This information is presented in Table 13.

Table 13. Mutually Soluble Binaries

Binary	Solubility Limits at 1366 K (weight percent)		Eutectic Temp (°C)	Comments
	A:B	B:A		
Au-Co	8.4	6	997	Au not compatible with Na
Au-Cu	M	M	911	Au not compatible with Na
Au-Pd	M	M	Lm-1064	Au not compatible with Na
Au-Pt	M	M	Lm-1064	Au not compatible with Na
Au-Ni	M	M	954	Au not compatible with Na
Cu-Co	8.8	13	Lm-1084	Low, high temperature strength
Cu-Pd	M	M	Lm-1084	Low, high temperature strength
Cu-Pt	M	M	Lm-1084	Low, high temperature strength
Cu-Ni	M	M	Lm-1084	Low, high temperature strength
Pd-Pt	M	M	Lm-1554	Melts too high
Ni-Pd	M	M	1239	Melts too high
Pt-Co	M	M	Lm-1495	Melts too high
Pd-Co	M	M	Lm-1219	Possible
Ni-Co	M	M	Lm-1455	Melts too high
Ni-Pt	M	M	Lm-1355	Melts too high

Lm - lowest melt temperature

The only binary in Table 13 that shows promise for this application would be Pd-Co.

Consideration can also be given to intermetallic forming elements that form eutectics, if the diffusion rate into the nickel is high. This can allow for dilution of the intermetallic phases with little impact on joint ductility. Elements such as B and P can be considered and can be coupled with soluble elements to form low melting eutectics (Table 14).

Table 14. Low Solubility Eutectic Binaries

Binary	Solubility Limits at 1366 K (weight percent)		Eutectic Temp (°C)	Comments
Mn-Ni	92	3	1020	Possible
Si-Ni	0	8	967	Possible
Ti-Ni	10	10	943	Possible
V-Ni	17	38	1205	Low diffusion rate
Zr-Ni	2	2	901	Possible
B-Ni	0	0	1093	Possible
P-Ni				Possible
Hf-Ni	1	1	1150	Possible
B-Co	0	0	830	Possible
B-Pd	3	34	900	Possible

Oxide vapor pressure data was gathered to estimate what elements might cause wetting problems for a Udimet 720 bond at 1366 K (see Table 15). This data shows which elemental oxides are the most likely to be removed by vaporization in two environments (1E-5 torr vacuum and inert gas).

Table 15. Oxide Stability

Element	Oxide Vapor Pressure at 1366 K (torr)	Vacuum	Inert-Gas
Al	< 5.0E-5	no	no
Au	> 1	yes	yes
Be	< 5.0E-5	yes	no
Cb	9.0E-3	yes	no
Cu	> 1	yes	yes
Co	> 1	yes	yes
Fe	> 1	yes	yes
Mn	0.05	yes	no
Mo	> 1	yes	yes
Pb	> 1	yes	yes
Pd	> 1	yes	yes
Pt	> 1	yes	yes
Re	> 1	yes	yes
Rn			
Si	5.0E-3	yes	no

Element	Oxide Vapor Pressure at 1366 K (torr)	Vacuum	Inert-Gas
Sn			
Ta	2.0E-2	yes	no
Ti	< 5.0E-5	no	no
V	8.0E-3	yes	no
Zn	> 1	yes	yes
Zr	< 5.0E-5	no	no
Ni	> 1	yes	yes

Yes - oxide is likely to be removed
No - oxide is not likely to be removed

A review of Table 13 shows the Pd-Co binary of the mutually soluble combinations to be the only candidate. The melting point of the Pd-Co system is 1219 °C which would be too high for the Udimet 720 since one normally joins at least 50 °C above the eutectic to ensure flow. This would make the bonding temperature 1269 °C, but the eutectic melt temperature of the Udimet 720 is 1250 °C. Almost all of the binaries listed in Table 14 were considered candidates based on their melting characteristics. However, the data presented in Table 12 was not complete enough to determine whether diffusion rates of those binaries forming intermetallics would be sufficient to dilute phases which result in bond embrittlement. In fact, tests run on Si, Mn, and Ti binaries with nickel all showed intermetallic phase formation in the bond joint (reference 8) which results in very low bond joint toughness.

Tests run at GFSD with B-Ni, and to a lesser degree with P-Ni, have shown greater joint toughness due to a greater dilution and distribution of the intermetallic in the base alloy matrix than with the Si, Mn, and Ti binaries. For this reason, the most promising binaries are B-Ni and P-Ni.

5.2.1.2 Literature search

A literature search was conducted by Nerac Inc. of Toliand, Connecticut under the direction of GFSD. The key words used in the search were "brazing" and "nickel-base superalloys." Nine files were searched which produced 318 abstracts as presented below:

Weld-A-Search	75
Engineering Meetings	20
CA Search-Applies	17
World Aluminum Abstracts	8
USG/NTIS	19
NASA	50
Mechanical Engineering	3
Engineering Index	51
Metal Abstracts	75

A review of the abstracts showed eight of the articles related directly to TLPDB and alternative joining methods on nickel-base superalloys. A discussion of the information in those articles that has application to this work is presented. A list of all titles found in the literature search are presented as Section 7, Appendix 2.

The most common systems used for TLPDB processing were the Ni-P and Ni-B binaries. These binaries have melting characteristics within the heat-treating constraints of the nickel-base superalloys (Figure 13).

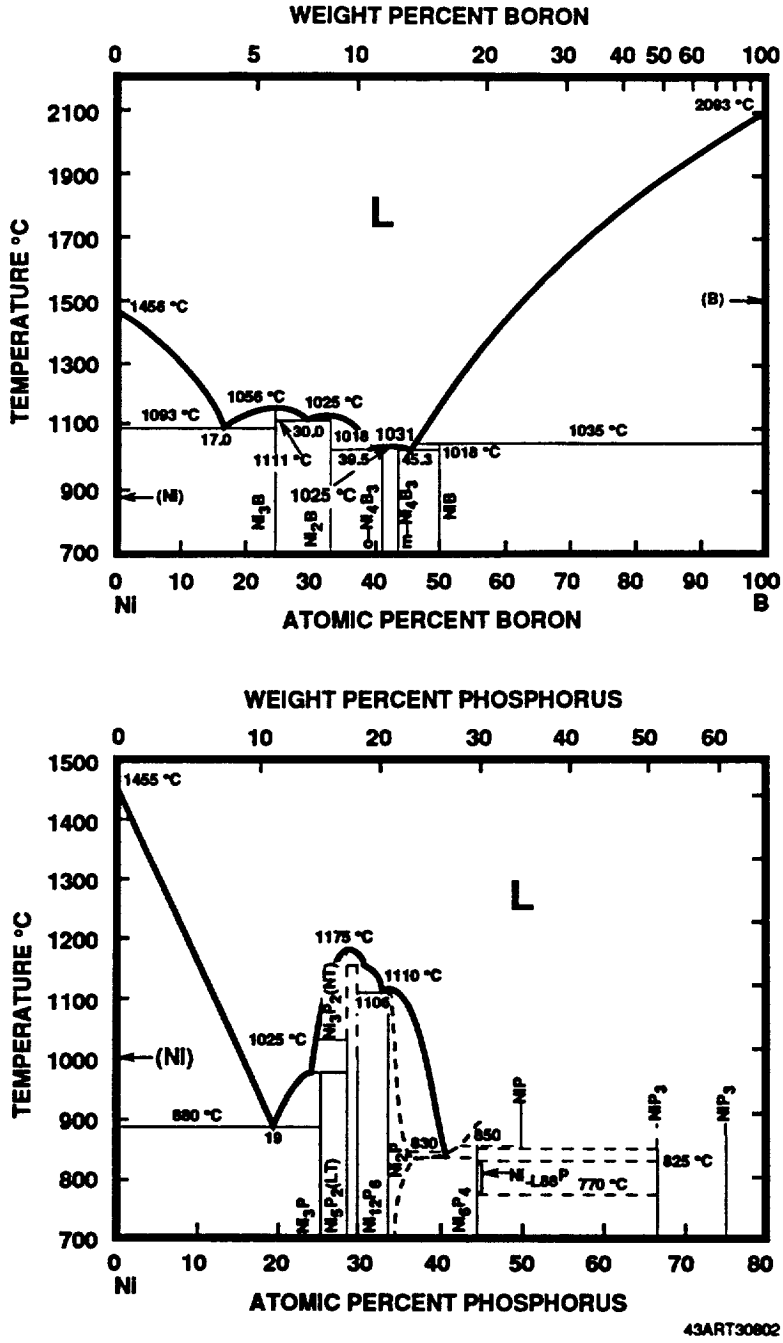

Figure 13. Ni-B and Ni-P Phase Diagrams

Both systems have steep liquidus lines which will allow for isothermal solidification. Work conducted at GFSD has shown the Ni-P system does show lower diffusion characteristics than the Ni-B system. This results in a greater tendency for formation of stable intermetallic phases in the bond joint region with the phosphorous system than with the boron system.

Other systems discussed in the literature used Si, Mn, Cb, and Ti binaries with nickel; however, unwanted stable intermetallic phases were reported to have formed in the bond interface region (reference 8). It seems reasonable, therefore, to downselect to a system with a boron melting point depressant based on the literature and the results of the phase diagram study.

Since the mechanical property requirements of the Stirling power converter application are quite high, some attention must be given to the strengthening mechanisms of the Udimet 720 system. This alloy uses gamma and gamma prime precipitation strengthening which is based on intermetallic phase formation from aluminum and titanium concentrations. The morphology, size, and quantity of these phases in the bond region ultimately determine the joint efficiency (reference 8). Work conducted on strengthening mechanisms on Udimet 700 has shown that bonding temperatures used below the gamma-gamma prime solvus result in a continuous layer of gamma prime at the bond interface which leaves no ductility or toughness in the bond region (reference 9). This is complicated by the fact that the solvus temperature for the alloy substrate and the two element interlayers may be quite different. In fact, cobalt additions to the Ni-B system of up to 20 percent will raise the gamma prime solvus to close to that of Udimet 700 resulting in solid solution diffusion of the aluminum and titanium from the base alloy to the bond region (reference 9). It is important that the gamma-gamma prime formers diffuse into the bond region. However, tests on Udimet 700 joints made with TLPDB have also shown that joint homogenization of all elements is directly related to joint efficiency (reference 8). Homogenization is related to concentration gradients, time at temperature, bond temperature, and thickness or diffusion distance (reference 8), as described in Fick's law (reference 10). The most promising interlayer would be one closely matched in composition to the solid solution elements of the parent material. This allows for diffusion in the solid state of intermetallic strengthening phases of the base material to the bond interlayer and dilution of a boron melting point depressant into the base material. After heat treatment, the precipitation of strengthening phases should be similar in size and distribution to those of the parent material.

Since boron interacts with elements such as Al, Ti, and W, the melting character of a Udimet 720 interlayer and the resultant intermetallic phases may not be consistent with TLPDB constraints and high joint efficiencies. The melting character of bond aid materials for TLPDB with Cr, Co, Mo, B, and Ni has been shown to be consistent with the constraints of the Udimet 700 alloy (reference 8), and would also be appropriate for use with Udimet 720. Experiments conducted on Udimet 700 with a bond aid interlayer with the following composition

Cr	Co	Mo	B	Ni
15	15	5	3.0	bal

showed no composition differences in the joint from the parent material after a 24-hour soak at 2140 °F (reference 8). This interlayer was 0.003-inch thick and the analysis was done with an electron microprobe.

Mechanical property testing on nickel-base superalloys at high and low temperatures in low cycle fatigue, tension, and stress-rupture has shown that TLPDB joints show the lowest joint efficiency in stress-rupture. This is directly related to joint homogenization (reference 8). Theoretical work done by Ikawa, Nakao and Isai has shown a relationship on homogenization of the elements that allows the design of a joint to produce high stress-rupture properties (reference 11). The following equation is used to calculate composition change in nickel alloys as a function of bond interlayer thickness, time at temperature, and temperature (reference 11). The temperature variable is incorporated into the diffusion coefficient of the solute atom.

$$c(t) = C_o \left(1-\mathrm{erf}\left(h/2(Dt)^{1/2}\right)\right) + C_i \qquad (1)$$

where $C_o = C_b - C_i$

C_b = solute atom concentration of base metal
C_i = initial solute atom concentration at the bonding layer
D = diffusion coefficient of solute atom
h = half thickness of initial bond layer

This equation can be used to calculate the maximum thickness of an interlayer that can be used to achieve joint homogenization and still meet the grain size constraints of the subject bond statement. This can be done with data from GFSD and the literature on homogenization times and temperatures by determining the diffusion coefficient for the slowest diffusing element.

The literature also revealed that Pratt and Whitney Aircraft Company has used TLPDB in production to join turbine vanes fabricated from nickel-base superalloys. The yield of the process was reported to be greater than 99.8 percent (reference 8).

5.2.1.3 Liquid-phase system selection

The work presented in the literature search discussion suggests that selecting an alloy with the solid solution elements Cr, Co, Mo, and Ni mixed with the melting point depressant B would maximize the chances of a homogeneous bond joint and lead to high joint efficiency. In addition, the intermetallic solvus would be similar in the interlayer allowing for solid solution diffusion of the Al, Ti, and W and proper precipitation distribution from the age heat treatment. This work is consistent with the results of the binary phase diagram study, which led to the use of a P or B system.

A search was conducted to locate an available braze alloy that may be close to that of the Udimet 720 alloy. A list of braze alloys available is presented in Table 16. No product was identified that was a boron depressant alloy similar to Udimet 720.

Table 16. Nickel-Base Braze Alloys Available in Foil or Powder Form

Alloy	Cr	Co	Mo	W	Ti	Al	Fe	Si	B
Udiment 720	18.0	14.7	3.0	1.25	5.0	2.5			
Met 75/75	10.0	23.0	7.0				5.5		3.5
Met 80/80	15.2								4.0
Micro L.M.	7.0						3.0	4.5	
Micro 150	15.0								
Metco 18C	18.0	40.0	6.0				2.5	3.5	3.0
Metco 15E	17.0							4.0	3.5
Met 90/90A		20.0						4.0	2.7
Proposed	18.0	15.0	3.0						3.5

Additional industry inquiries revealed that Union Carbide can make powders in various compositions based on nickel. The following alloy was identified as consistent with TLPDB needs for Udimet 720 and could be made by Union Carbide:

Cr	Co	Mo	B	Ni
18	15	3	3.5	bal

Work would be needed to determine the exact melting characteristics with adjustments in the B concentration to place the liquidus at approximately 2100 °F or below.

5.2.1.4 Cleaning and Coating Study

When considering the surface preparation of the mating parts, the joint fit requirements, as related to asperities that the bond aid liquid must fill, need to be determined. The fit would, therefore, be a function of the bond aid thickness. The minimum bond aid thickness that has been successful with regard to manufacturing surface preparation capabilities is 100 micro-inches per surface. Bond aid thicknesses less than 75 micro-inches per surface will not allow for the formation of new grains during isothermal solidification. GFSD has determined that a surface finish of 32 micro-inches and parallelism of 0.002 inch per inch is required with a 100 micro-inch bond aid thickness with no parent material distortion during bond.

The bond aid thickness selected is primarily a function of diffusion time and temperature required for homogenization and manufacturing capability. Longer times or higher temperatures are required for the thicker bond layers. Both higher temperatures and longer times will result in additional grain growth of the parent alloy. Therefore, thin bond aid layers are desirable in the Stirling power converter application.

In an effort to determine the thickest bond aid layer, one needs to consider the grain size limitations of this application. Examination of the grain size requirements listed in Table 9 shows that the pacing limitation for this application is the limit of ASTM 4-6 for Inconel 718 and limit of ASTM 8-10 for Udimet 720. The TLPDB soak time will be determined by the grain size limitation.

A calculation of the Udimet 720 grain growth during the TLPDB process has been performed using the relationship

$$D^2 - D_o^2 = K_o t e^{-Q/RT} \qquad (2)$$

where,
D = final grain size
D_o = starting grain size
K_o = grain growth constant
t = time
Q = activation energy
R = gas constant
T = temperature

Experiments conducted by GFSD on Udimet 720 have shown that with a starting grain size of ASTM 9, after a 2200 °F soak of 4 hours, the final grain size is ASTM 6 (see Figure 14). The grain growth constant, K_o, and activation energy, Q, of equation 2 were determined from this experimental data, and calculations were made to determine the required starting grain size on the Udimet 720 to achieve a final grain size of ASTM 8. Assuming a thermal cycle of 2140 °F for 4 hours, the initial grain size required is ASTM 11.

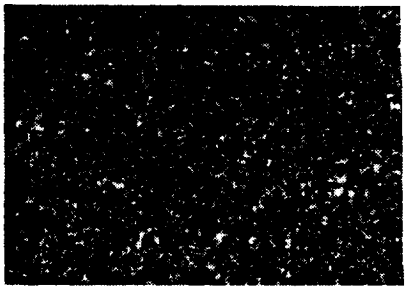

ASTM No. 9
Starting Condition

ASTM #6
Final Condition

Vacuum Thermal Cycle (2200 °F for 4 hours)

Figure 14. Grain Size Experiment for Udimet 720

For Inconel 718, the values of K_o and Q were also determined from GFSD data. Assuming a starting grain size of ASTM 10 and a thermal cycle of 4 hours at 2140 °F, the final grain size is ASTM 4. Equation 1 can then be used to calculate the maximum interlayer thickness with this thermal cycle that would achieve joint homogenization. The following data were used in the calculation:

- Data from the literature on the homogenization concentrations for Udimet 700
- The diffusion coefficient for Al into Ni
- The thermal cycle temperature and time from the grain size limitation calculation above (4 hours at 2140 °F).

The maximum total thickness based on this calculation is 0.001 inch. Therefore, any thickness between 200 micro-inches (100 micro-inches per surface) and 0.001 could be thermally processed within the grain size constraints of this application.

Two hundred micro-inches was selected as a minimum thickness based on GFSD experience with flatness and surface finish related to filling any bond asperities. Thin bond aid layers are commonly used for production TLPDB at GFSD in bonding intricate fluidic laminates. The maximum thickness of 0.001 inch was calculated based on grain growth limitations and theoretically should homogenize with the recommended thermal cycle. However, to ensure homogenization, thicknesses close to the minimum are recommended.

The 32 micro-inch finish that has been used at GFSD is achieved with grinding and lapping operations. Abrasive grinding must be avoided to prevent excessive oxidation of the surface. Prior to coating, bond surfaces are vapor degreased in 1,1,1-trichloroethane, followed by cold methanol, and blow dried. This step can also be done with vapor degreasing in Freon TA. Inconel 718 can then be etched in a HNO_3/HF solution for 2 minutes to remove any oxides or remaining contaminants. Udimet 720 most likely will etch in a ferric chloride solution based on experience with Rene 41. Parts are then handled with gloves and coated within 4 hours of cleaning.

The bond aid material choice is an alloy similar in composition to Udimet 720 using boron as a melting point depressant with no elements that form intermetallics (e.g. aluminum or titanium). Since this alloy will contain more than two elements, electroplating is eliminated as a possible coating method. Plating is normally limited to binary compositions.

Other chemical methods such as chemical vapor deposition (CVD) are also limited to one or two element depositions. Mechanical and physical coating methods such as painting, plasma spray, and sputtering are better suited to applications such as this with complex alloy compositions.

The paint method uses a powder of the bond aid alloy that is mixed with a liquid organic binder. The binder dries after spray application forming an adherent film. The binder is then burned off during the thermal cycling part of the TLPDB process. The metallic paint process is limited by how effectively the binder can be burned off and by the particle size available in the powder. The powder mesh sizes available from Union Carbide do not appear to be consistent with this process to achieve very thin layers such as 100 micro-inches.

Another possible method is the plasma spray method. This is done in a vacuum chamber to prevent oxidation of the bond alloy during spray. The process uses a powder which is heated and accelerated at the substrate in a spray. The material bonds to the substrate by a mechanical interlock. This is a relatively clean process, however, thickness is limited to the particle sizes available. A thermal spray alloy has been identified with a composition similar to that required for this application. Metco 18C was considered as a bond aid candidate. It is available in 140 mesh powder. This coating method uses roughly spherical particles which deform to slivers when applied to the bond surfaces. Since the coating is not fully dense, some development would be required to determine what initial thickness would give the required thickness after melting. Vendor consulting suggested that 500 micro-inches would be achievable. Braze powders may also be thermal sprayed. Metco and Special Processes of Arizona were consulted on this effort.

The final method considered was sputtering. This method is conducted in a vacuum chamber where a target of the bond aid alloy is struck with a beam of charged argon. This produces a mist which deposits onto the substrate. The resultant coating morphology is fine grained, high density, very pure, and free from contamination. In addition, the bond surfaces can be cleaned in the sputter chamber by striking the surface with the beam. This process requires a target of the bond aid alloy which has not been found to be currently available. However, sputtering targets can be made from powders by hot pressing or by vacuum plasma spray. Thin Film Technology and Coating Technology were consulted and they can vacuum spray, sputter, and fabricate the sputter targets.

Since the sputtering process offers the ability to apply complex compositions in very thin layers and surface oxides can be removed in a vacuum chamber prior to coating, this process is selected for use on the Stirling application.

5.2.1.5 Bonding Scheme Definition

The process of TLPDB has five basic steps required to make a high-strength bond joint. They include surface preparation, coating application, assembly, thermal processing and heat treatment. Each step will include several sub-steps that will affect the quality of the final bond joint. Table 17 shows the processing parameters presented in the sequence they would be conducted with the associated end item effects.

Table 17. Processing Parameters and Related Effects

Step	Variables	End Item Effect
1) Surface prep	a) Cleanliness	Voids
	b) Surface finish	Voids, IJR*
	c) Surface flatness and parallelism	Voids, IJR
2) Coat bond surfaces	a) Deoxide	
	• Etch time	Voids
	• Sputter time	Voids, IJR
	b) Apply bond aid alloy	
	• Coating uniformity	IJR
	• Thickness	IJR, dilution of beta, low creep, homogenization, substrate grain growth, excess flow
	• Alloy mix	No melt, low creep, brittleness
3) Assembly	a) Cleanliness	Voids
	b) Joint fit	No bond
4) Thermal cycle	a) Load profile	Voids, IJR, excess flow
	b) Ramp up	IJR, no melt
	c) Soak time	Brittleness, low creep, dilution of B, substrate grain growth, IJR, homogenization
	d) Atmosphere	Voids
	e) Soak temperature	No melt, low creep, brittleness, IJR, substrate grain growth
	f) Ramp down	
	g) Temp measurement	
	h) Stop offs	Voids
5) Heat treatment	Since the final heat treatment condition is specified and the heat treatment is performed after bonding, the bonding process must yield homogeneous materials to allow proper heat treatment.	

*IJR - incomplete joint recrystallization

The surface preparation must be done in a manner to avoid contamination such as grit, oils, and metal compounds (especially oxides) since the cleanliness of the surface onto which the coating is applied will affect wetting and the basic ability to achieve a diffusion bond without defects or voids. The surface conformance at the bond interface needs to be within the interlayer material thickness or incomplete joint recrystallization (IJR) and bond line voids will result.

The bonding environment must be consistent with preventing the reaction of gasses with the subject metal elements at bonding temperature. In addition, there is value in a bonding atmosphere that will remove oxides of metals which were not adequately cleaned. This process can occur in a vacuum by sublimation. Based on the elements contained in Udimet 720 and information presented in Table 15, one can conclude a vacuum level below 1.0E-4 torr would be sufficient except for Al and Ti. The oxides of Al and Ti should be removed, however, during the sputter coating operation.

The bond process variables were reviewed and separated into two categories, controlled and adjustable, as shown in Table 18.

Table 18. Bond Parameter Category

Controlled	Adjustable
Cleanliness	Surface finish
Atmosphere	Conformance
Deoxide	Bond aid thickness
Alloy mix	Load profile
Assembly	Ramp up
Stop off	Soak time
Bond aid application	Soak temperature Boron concentration

Based on the literature and GFSD experience, the limits for the adjustable parameters were identified and are listed in Table 19. These parameters can then be varied in physical experiments to determine the optimum values for the properties required for the Udimet 720/Udimet 720 joints and Udimet 720/Inconel 718 joints.

Table 19. Process Parameter Limits

Variable	Parameter Limits	
Surface finish (micro-inch)	32	64
Surface conformance (in/in)	0.002	0.004
Total bond alloy thickness (in)	0.002	0.0004
Bond alloy boron concentration (percent)	2.5	3.5
Load profile (psi)	50	100
Temperature ramp rate (°C/min)	20	30
Soak time (hours)	4	6
Soak temperature (°F)	2100	2150

5.2.1.6 TLPDB Test Plan Development

In an effort to determine the strength of a process variable with regard to the end item effect and to minimize the number of tests required, a Taguchi statistical analysis was conducted. The analysis was performed based on known physical effects of process variable changes and variable interactions. These relationships are presented in Table 20.

Table 20. Process Variable Versus Physical Effect

No.	Variable	Physical Effect	Affected Variables
1	Surface finish	A,B	3,5
2	Surface conformance	A,B	3,5
3	Bond alloy thickness	B	1,2,5,7,8
4	Bond alloy B conc.	B,C,E,F	6,8
5	Load profile	A,F	1,2,3
6	Ramp rate	B,E	4
7	Soak time	C,D,G	3,8
8	Soak temperature	B,C,D,F,G	3,4,7

A Bond interface voids
B Incomplete recrystallization
C Dilution of boron
D Elemental homogenization
E No melt
F Excess flow
G Excessive grain growth

The Taguchi analysis is presented in Table 21 and 22 which shows that 16 tests are required based on parameters presented in Table 19 to arrive at the optimum process.

Table 21. TLPDB Taguchi Analysis

LIQUID PHASE DIFFUSION BONDING

STIRLING MATERIALS TECHNOLOGY PROGRAM

LARGER THE BETTER-LB
SMALLER THE BETTER-SB
NOMINAL THE BEST-NB

DATE: 09/16/91
FILE: BOND3_TGU.WK1

L16

FACT TEST	A BOND ALLOY CONC	B RAMP RATE C/MIN	C A X B	D SOAK TIME HRS	E SURF FINISH	F BOND ALLOY THICK	G (OPT)	H SOAK TEMP C	I (OPT)	J LOAD PROF PSI	K SURF CONF IN/IN	L D X H	M F X K	N (OPT)	O E X J
1	2.5%	20		4	32	.0002		2100		50	.002				
2	2.5%	20		4	32	.0002		2150		100	.004				
3	2.5%	20		6	64	.0004		2100		50	.002				
4	2.5%	20		6	64	.0004		2150		100	.004				
5	2.5%	30		4	32	.0004		2100		100	.004				
6	2.5%	30		4	32	.0004		2150		50	.002				
7	2.5%	30		6	64	.0002		2100		100	.004				
8	2.5%	30		6	64	.0002		2150		50	.002				
9	3.5%	20		4	64	.0002		2100		50	.004				
10	3.5%	20		4	64	.0002		2150		100	.002				
11	3.5%	20		6	32	.0004		2100		50	.004				
12	3.5%	20		6	32	.0004		2150		100	.002				
13	3.5%	30		4	64	.0004		2100		100	.002				
14	3.5%	30		4	64	.0004		2150		50	.004				
15	3.5%	30		6	32	.0002		2100		100	.002				
16	3.5%	30		6	32	.0002		2150		50	.004				

Table 22. TLPDB Taguchi Analysis Results Form

LIQUID PHASE DIFFUSION BONDING RESULTS

DATE: 09/16/91

STIRLING MATERIALS TECHNOLOGY PROGRAM

FILE: BOND3_TGU.WK1

LARGER THE BETTER-LB
SMALLER THE BETTER-SB
NOMINAL THE BEST-NB

L16 ***RESULT TABLE***

TEST #	SB BOND INTERFACE VOIDS	LB RECRYSTAL-LIZATION NEW GRAINS	SB DILUTION OF BORON	SB ELEMENTAL HOMOGENI-ZATION	LB TENSILE (RT)	LB CREEP/ RUPTURE	LB NO MELT	SB EXCESS FLOW FILLETS	SB GRAIN GROWTH (ASTM)
1									
2									
3									
4									
5									
6									
7									
8									
9									
10									
11									
12									
13									
14									
15									
16									

5.2.1.7 TLPDB evaluation criteria

The inspection methods and acceptance criteria are given in Table 23 which is based on development experience at GFSD with this process and the end-item requirements of the Stirling bond joints.

Table 23. Test Matrix Criteria

Physical Effect	Inspection Method	Acceptance
Bond interface voids	Metallographic	No voids
Incomplete recrystallization	Metallographic	New grains
Dilution of boron	SEM/EDX/XRD	No detection
Elemental homogenization	SEM/EDX	No more than 2 percent
	Tensile (RT)	90 percent of parent
	Creep/rupture	90 percent of parent
No melt	Micro/visual	Must melt
Excess flow	Visual	Fillets only
Excess grain growth	Metallographic	See Table 9

SEM - scanning electron microscope
EDX - energy dispersive X-ray
XRD - X-ray diffraction

5.2.3 TLPDB Study Conclusions

A review of the requirements of the Stirling bonds suggests that TLPDB is ideally suited for this application. Problems with strain age cracking limit the use of more conventional joining techniques for the Udimet 720 joints of the Stirling power converter. For the TLPDB process, some development tests will have to be performed prior to practical application to Stirling hardware as outlined in the Taguchi matrix. These tests will ensure mechanical property conformance to application requirements.

The literature search identified many variables with regard to this process with nickel-base superalloys, but process development could be done quickly for nickel-base systems. In addition, information was available suggesting that TLPDB is a very reliable process, producing up to 99.8 percent yield on nickel-base superalloys.

The critical variables in TLPDB are the proper selection of a bonding aid interlayer and thickness, bonding aid application method, bonding time, temperature and load, and geometrical conformance. All of these variables were identified in regard to TLPDB of Udimet 720.

5.3 Liquid-Metal Compatibility

5.3.1 Liquid Metal Compatibility Analysis

The design and application of most high-temperature engineering systems are limited primarily by the properties of the materials available for construction. In no case is this fact more apparent than in liquid-metal heat-transfer systems which are limited by the properties of suitable containers and structural materials. These properties include such concerns as mechanical strength, dimensional stability, heat-transfer characteristics, fabrication details and, specifically, the ability to withstand attack by liquid metals.

System temperature differentials along with a variation of solubility with temperature can lead to corrosion of pipes and vessels containing liquid metals. From experience, it has been determined that mass transfer in liquid metal systems follows the same correlations as in non-metals. It has been established that surface oxide films inhibit wetting of metal

surfaces. On the other hand, with well-wetted metal surfaces, there is no surface or chemical transfer resistance to assist the usual liquid phase transfer resistance to the corrosion process.

Mass transfer from the solid to the liquid metal is controlled by solid-phase diffusion and cannot be predicted from correlations based on liquid-phase diffusion. The fundamental transfer mechanism is unaltered by the system geometry.

The possibility of diffusion bonding or self-welding of solid metal surfaces to each other and thus interfering with the operation of valves, pumps, and flanged joints could be a factor in determining the upper temperature limit of operation of a liquid-metal heat transfer system. Such self-welding is facilitated by contact with an alkali metal, is intensified if the metals are held together under pressure, and becomes increasingly serious with increasing temperature.

5.3.1.1 Compatibility

The liquid metals of interest in this study are the alkali metals lithium (Li) and sodium (Na), and the sodium-potassium alloys (NaK). For a 1050 K SP-100 Stirling power system design for a lunar base, lithium is used to transport the heat input from the reactor to the Stirling power converter. Two lithium loops are used in series with an intermediate heat exchanger between them. The maximum temperature in the lithium loop delivering the heat to the Stirling power converter is estimated to be at about 1115 K. A sodium heat pipe then transfers the heat input to the helium working fluid within the power converter. The sodium vapor temperature is expected to be about 1060 K. The Stirling converter hot-end temperature is defined to be 1050 K at the helium-side wall temperature of the heater. Finally, NaK is used to transport the rejected heat from the power converter to the radiator. The maximum NaK temperature is estimated to be about 530 K.

As a group, the alkali metals are more uniform in physical and chemical properties than any other family of elements. They are very reactive chemically and the reactivity increases with increasing atomic weight. They are all strong reducing agents and readily form univalent positive ions.

Lithium is the least dense of the normally solid elements and it is the least typical and the least reactive of the alkali metals. There is a single electron in the outermost shell of the alkali metals, which is easily lost since this electron is far removed from the rest of the atom. Therefore, all of the alkali metals readily form stable positive ions. The ease with which the valence electron is lost increases with increasing atomic radius. Lithium has the smallest atomic radius of the alkali metals. Molten lithium reacts with all known molecular gases. Lithium melts at 179 °C (354 °F) and boils at 1317 °C (2403 °F).

The most prominent characteristic of molten sodium is its reactivity with most gases or liquids other than the noble gases and nitrogen. The reaction of sodium in contact with the atmosphere is of great importance in that the end product after heating is Na_2O which results in a considerably increased attack on metal surfaces. Sodium melts at 97.8 °C (208 °F) and boils at 883 °C (1621 °F).

Sodium-potassium alloys are liquid at room temperature from 40 to 90 weight percent potassium. The liquid alloys are more reactive than either component at the same temperature but otherwise behave as the alkali metals in general. Like sodium and the heavier alkali metals, NaK does not react with nitrogen.

5.3.1.2 Corrosion

Liquid-metal corrosion may take place by several fairly common mechanisms. One is a relatively uniform solution attack on the solid surface by the liquid corrodant. Another common method of attack is direct alloying, that is, the interaction between liquid and solid to form surface films or typical diffusion layers of intermetallic compounds and solid solutions. These may form loosely adherent scale or, if held tightly, may serve as a barrier to slow down additional diffusion.

The rate of corrosive attack on metal surfaces by liquid metals may vary significantly with flow rate if the slowest step in the corrosion process is the rate at which solute

diffuses through the liquid boundary film. On the other hand, the corrosion rate may be independent of the flow rate if the slow step is the rate of dissolution of the solid or the rate of diffusion in the solid phase.

Corrosion can also occur as a result of contaminants such as oxygen, nitrogen or carbon in the liquid metal. As in the case of alloy layers, a metal oxide layer, for example, is sometimes tenacious and adherent and acts as a diffusion barrier; in this case, it inhibits further attack. Conversely, it may be non-adherent, in which case drastic weight loss occurs, especially under dynamic conditions.

Erosion corrosion results from mechanical attack by flowing or turbulent liquid metal and involves the removal of scales or films, abrasion by suspended particles or, in extreme cases, cavitation.

Of particular interest in liquid metal systems is a type of mass transport, thermal-gradient transfer, which is due to the co-existence of a temperature differential and an appreciable thermal coefficient of solubility. Even though the actual solubility may be quite low, large amounts of a solid component may be dissolved from the zone of higher solubility and precipitated in the zone of lower solubility. This continuing removal of the dissolved component from the system accelerates corrosive attack in some areas, while the precipitated material accumulates in the other parts of the system and may eventually cause plugging of the flow channels. In certain cases, the net thermal-gradient mass transfer of a pure metal phase from a hot zone to a cold zone may proceed by way of the formation of an intermediate chemical compound in the dissolution step. For example, it is believed that sodium oxide, dissolved in liquid sodium, may react with iron in a hot zone to form a compound containing iron, sodium and oxygen. This compound may then revert to sodium oxide and free iron in a cold zone and thus cause a net transport of metallic iron.

Another type of mass transfer from one part to another of a multi-metallic system, concentration-gradient transfer, may be encountered even in an isothermal system. Instead of the dissolving of one metal stopping when the liquid is saturated, the equilibrium may be upset by the presence of a second metal. This second metal can alloy with the dissolved metal to form solid solutions or compounds by precipitation or in a surface diffusion layer. An alloy layer thus formed may act as a diffusion barrier, causing the mass transfer rate to decrease with time.

In the case of liquid alkali metals, the presence of dissolved oxygen or oxides (and dissolved nitrogen or nitrides in the case of lithium) renders the fluid more corrosive. This enhancement of the corrosivity may result from dissolved compound formation as discussed previously, or it may affect the surface-fluxing ability of dissolved oxides, i.e., the tendency of dissolved oxides to remove protective oxide films from the metal surface. This problem may be minimized in practice by removing oxide contaminants or solids in a trap which allows the molten metal to cool near its freezing point in the presence of suitable precipitation sites. In addition, certain metals, such as the alkaline earths, when used as additives, may reduce the corrosivity of the alkali metals by selectively consuming oxygen. Alternately, the liquid metal may be continuously stripped of oxygen by exposing it to more easily oxidized metals, such as titanium or zirconium, in hot gettering traps. In the use of these two different type of oxygen getters, the mechanisms are the same, i.e., corrosivity is reduced by selectively consuming oxygen. The methods are different: in the case of the alkali earths, oxygen getters are simply added to the liquid metal itself while in the case of titanium and zirconium, a continuous oxygen getter is part of the overall system.

5.3.1.3 Embrittlement

Selective reaction of the liquid metal with minor constituents of the solid may result in inter-granular penetration or in the depletion of a dissolved component of the solid. Selective grain-boundary attack can drastically alter the physical properties of a material without appreciably changing its weight or appearance. The result is liquid metal embrittlement or grain fallout. This type of attack is often accelerated by the application of stress to a solid during exposure to the liquid metal.

5.3.1.4 Experience

Austenitic stainless steels, nickel and nickel-base superalloys such as Inconel 718 and Udimet 720, cobalt and cobalt-base alloys, chromium and the refractory metals columbium, molybdenum, tantalum, tungsten and their alloys should all be compatible with liquid sodium

and NaK up to the maximum design temperatures. The vast majority of the sodium and NaK containment experience reported in the literature to date has been with the austenitic stainless steels. There appears to be no difference in performance of stabilized grades versus non-stabilized grades. Many mixed metal systems have been built and operated successfully. Although mass transfer between some metals has been observed in laboratory tests, the materials which have ordinarily been used in system construction, i.e., several varieties of stainless steels including ferritics, nickel, and nickel-base alloys (Inconels), have shown little tendency for mass transfer. However, one should not conclude that these alloys will work in any liquid sodium or NaK system, but may be used as a starting point for materials testing.

With regard to the effect of sodium or NaK on brazements, the behavior of a brazed joint can be deduced from the behavior of the braze metal or the major constituents of the brazing alloy. For instance, silver or gold brazes have absolutely no resistance to corrosion in liquid sodium or NaK as would be expected from the limited corrosion resistance of silver and gold. Among those brazing alloys which are resistant to sodium and NaK are high chromium-nickel alloys and chromium-nickel-silicon alloys.

No accounts of preferential attack of austenitic stainless steel welds in Na or NaK was found in the literature. The commercially available stainless welding rods form joints which are as resistant to corrosion as the base metal. There is no special susceptibility developed in the heat-affected zones. From the standpoint of system cleanliness and subsequent sodium purity, it is desirable to avoid joints where large quantities of welding slag can be trapped because this slag may later be leached out. Welded joints of other potential materials, such as nickel-base and cobalt-base alloys, would also be expected to have corrosion behavior similar to the base metals.

For containment of liquid lithium, only austenitic stainless steels and the refractory metals columbium, tantalum, molybdenum and their alloys appear to be suitable for prolonged use. The austenitic stainless steels have been used successfully in lithium systems below 538 °C (1000 °F). The nickel-base and cobalt-base alloys appear to be inferior to the austenitic stainless steels for handling lithium. No significant differences between type 304 and the other 300-series stainless steels have been encountered in lithium service. Type 304 stainless steel reportedly has very low solution mass transfer rates in lithium. While welded stainless steel joints should withstand prolonged lithium exposure, brazed joints would probably be unacceptable because of the corrosion susceptibility of the braze alloy. Above 538 °C (1000 °F), the refractory metals and their alloys have shown relatively good resistance to lithium. These materials would be necessary for the lithium loops of the Stirling power systems.

5.3.1.5 Discussion

From this liquid metals compatibility study, it is evident that it is not possible to dependably predict system compatibility with liquid metals without thorough testing. Even though an impressive amount of data has been collected on the use of liquid metals, evaluation of liquid-metal compatibility in a complex system cannot rely solely on information in the literature. The number of factors which must be considered in designing a liquid-metal system tend to make each design unique. Such parameters as liquid-metal purity, environmental contamination, flow rates, flow channel geometry, temperatures, temperature gradients, and expected system lifetime, for example, tend to be design specific. The corrosion mechanisms discussed earlier may act independently or in various combinations in an actual liquid-metal system. Their effects may be additive, synergistic, or counteractive. Changing any of the design parameters could render the materials in a previously successful system susceptible to corrosion failure. For liquid sodium and NaK, the literature indicates that stainless steels, nickel and nickel-base alloys, cobalt-base alloys, and the refractory metals and alloys should be corrosion resistant to the maximum proposed design temperatures. However, because of design-specific details such as contaminants, flow rates, temperature gradients, and design lifetime which may or may not have been factored into the previous testing or evaluation of these materials, they should be viewed as candidate materials only.

For liquid lithium, the literature indicates that austenitic stainless steels are superior to the nickel-base and cobalt-base alloys up to approximately 538°C (1000°F). Above this temperature, the austenitic stainless steels are only recommended for short-term use. The refractory metals and their alloys should be acceptable to the maximum lithium temperatures for the Stirling power system (1115 K for the loop to the Stirling power

converter). Again, the conditions under which existing data have been collected are highly variable. System cleanliness and liquid-metal purity alone can have a dramatic impact on corrosion behavior and whether or not a metal is judged to be acceptable for use.

Acceptable system cleanliness and purity requirements are dependent on the other operating conditions such as temperature, flow rate, materials, expected life, etc. The greater the level of cleanliness and purity, the greater the flexibility in the other system parameters. It is not possible, therefore, to be specific as to the exact requirements that should be placed on cleanliness and purity.

Oxygen is by far the most serious contaminant in sodium or Nak systems and is one of the most important single factors affecting corrosion. Other impurities in sodium or Nak play minor roles in comparison to oxygen with regard to corrosivity. Simple stainless steel heat transfer systems using sodium or NaK have reportedly operated successfully with oxygen contents below 0.02 weight percent (144 ppm) up to 538 °C (1000 °F).

Very little data exists on corrosion as a function of contamination of lithium by impurities. Aside from oxygen, nitrogen in lithium has a major effect on corrosivity. Lithium nitride is a very reactive compound and no metal or ceramic material has been found to be resistant to the molten nitride. Oxygen is more often present in solid lithium as a hydroxide than an oxide. Molten lithium hydroxide is very corrosive and, again, no refractory or metal has been found suitable for handling it. Therefore, precise levels of liquid-metal purity, as determined by experimentation, must be maintained to eliminate problems associated with lithium nitride and lithium hydroxide contamination.

Although test results indicate that lithium is more aggressive in its corrosive attack on most metals than either sodium or Nak, the purity of the lithium used in most tests makes the results somewhat questionable. Most of the reported corrosion tests have used commercial-grade lithium of questionable and, certainly not consistent, purity.

5.3.2 Liquid metals recommendations

1. For liquid sodium or NaK systems, austenitic stainless steels, nickel-base alloys, cobalt-base alloys, and refractory metals and their alloys should be considered candidate materials up to the maximum design temperatures of 530 K (495 °F) for the NaK and 1060 K (1450 °F) for the Na vapor.

2. For liquid lithium systems, austenitic stainless steels should be considered candidate materials up to 811 K (1000 °F). Refractory metals and their alloys are candidates up to the maximum lithium temperature of 1115 K (1547 °F) for the loop to the Stirling power converter.

3. Nickel-base or cobalt-base alloys should be considered high-risk materials for use in lithium.

4. If austenitic stainless steels are to be considered for use above 811 K (1000°F) or if nickel-base or cobalt-base alloys are to be used at all in liquid lithium, static coupon tests should be conducted to determine viability as a candidate material.

5. All candidate alloys selected for use in lithium, sodium, or NaK should be tested under conditions which simulate expected operational systems as closely as possible. Such parameters as liquid-metal purity, environmental contamination, flow rates, flow channel geometry, temperatures, temperature gradients, and expected system lifetime should all be considered in establishing specific test conditions.

6. All liquid-metal systems must maintain the highest level of cleanliness and liquid-metal purity throughout the testing and evaluation of materials.

If a test matrix is considered to determine the interacting effects of the liquid-metal variables, then a Taguchi experiment may be useful to reduce the number of tests. The matrix presented in Table 24 shows the interactions of effect to liquid-metal parameters for sodium. Tables 25 and 26 show the results of the Taguchi analysis based on Table 24 indicating 16 tests are required if two variables are selected from each category (except liquid metal). Conducting this minimum number of tests will allow the experimenter to determine the interactive effects of parameters and which parameters have the strongest influence on the effect.

Table 24. Sodium System Variables

Variable	Number of Variable	Variable Limits	Effect	Analysis Method
Temperature	2	(X, Y)	SA, IGE, MT, CA	MET, SEM-EDX TT
Temperature gradient	2	(X, Y)	MT	SEM-EDX
Flow	2	(X, Y)	SA, IGE, MT, CA	MET, SEM-EDX TT
Contamination	2	(X, Y)	CA	SEM-EDX
Dissimilar metals	2	(ni, Fe)	MT	SEM-EDX
Stress level	2	(X, Y)	IGE	MET, TT
Liquid metal	1	(Na)	SA, IGE, MT, CA	MET, SEM-EDX TT

CA - Contaminant attack
IGE - Intergranular embrittlement
MET - Metallographic
MT - Mass transfer
SA - Solubility attack
TT - Tensile testing

Table 25. Liquid Metal Compatibility Taguchi Analysis

SODIUM SYSTEM TAGUCHI EXPERIMENT

DATE: 10/22/91
FILE: NASYS_TG.WK1

LARGER THE BETTER-LB
SMALLER THE BETTER-SB
NOMINAL THE BEST-NB

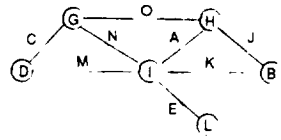

L16

FACT	A	B	C	D	E	F	G	H	I	J	K	L	M	N	O
	I X H	DISSIM METAL Ni, Fe	D X G	CONTAMI-NATION %	I X L	(OPT)	FLOW	TEMP GRADIENT	TEMP	B X H	B X I	STRESS LEVEL	D X I	G X I	G X H
TEST															
1		X		X			X	X	X			X			
2		X		X			X	Y	Y			Y			
3		X		Y			Y	X	X			Y			
4		X		Y			Y	Y	Y			X			
5		Y		X			Y	X	X			X			
6		Y		X			Y	Y	Y			Y			
7		Y		Y			X	X	X			Y			
8		Y		Y			X	Y	Y			X			
9		X		X			Y	X	Y			X			
10		X		X			Y	Y	X			Y			
11		X		Y			X	X	Y			Y			
12		X		Y			X	Y	X			X			
13		Y		X			X	X	Y			X			
14		Y		X			X	Y	X			Y			
15		Y		Y			Y	X	Y			Y			
16		Y		Y			Y	Y	X			X			

Table 26. Liquid Metal Compatibility Taguchi Analysis Results Form

SODIUM SYSTEM TAGUCHI EXPERIMENT

DATE: 10/22/91
FILE: NASYS_TG.WK1

LARGER THE BETTER-LB
SMALLER THE BETTER-SB
NOMINAL THE BEST-NB

L16 ***RESULT TABLE***

TEST #	SB SOLUBILITY ATTACK	SB INTERGRANULAR EMBRITTLEMENT	SB CONTAMINATION ATTACK	SB MASS TRANSFER					
1									
2									
3									
4									
5									
6									
7									
8									
9									
10									
11									
12									
13									
14									
15									
16									

6. CONCLUSIONS

Based on the technology review, it is recommended that changes in the power converter assembly sequence be incorporated to facilitate the use of TLPDB. In addition, it is recommended that further examination of alternative design concepts for the power converter bearings and heat exchangers be undertaken. The liquid-metal study indicates that compatibility testing should be performed under conditions which simulate expected operational systems as closely as possible. The TLPDB study shows that the technique can be applied to many joints in the Stirling power converter. Based on the alternative joining techniques study, TLPDB is recommended for all Udimet 720 joints. This program was limited to a theoretical evaluation of the TLPDB process for the Stirling power converter. It is recommended that the next step in the development of TLPDB for this application be demonstration of the process on sample coupons, prior to applying TLPDB to actual power converter hardware.

7. APPENDICES

Appendix 1. GLIMPS Simulation Plots

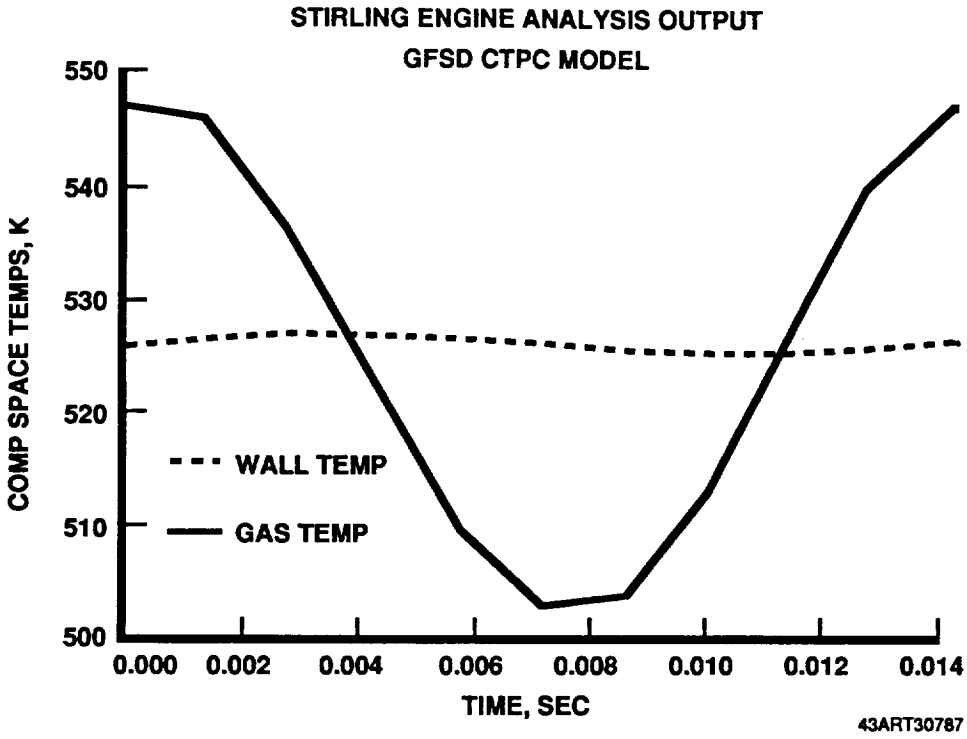

Figure 15. Compression Space Temperature

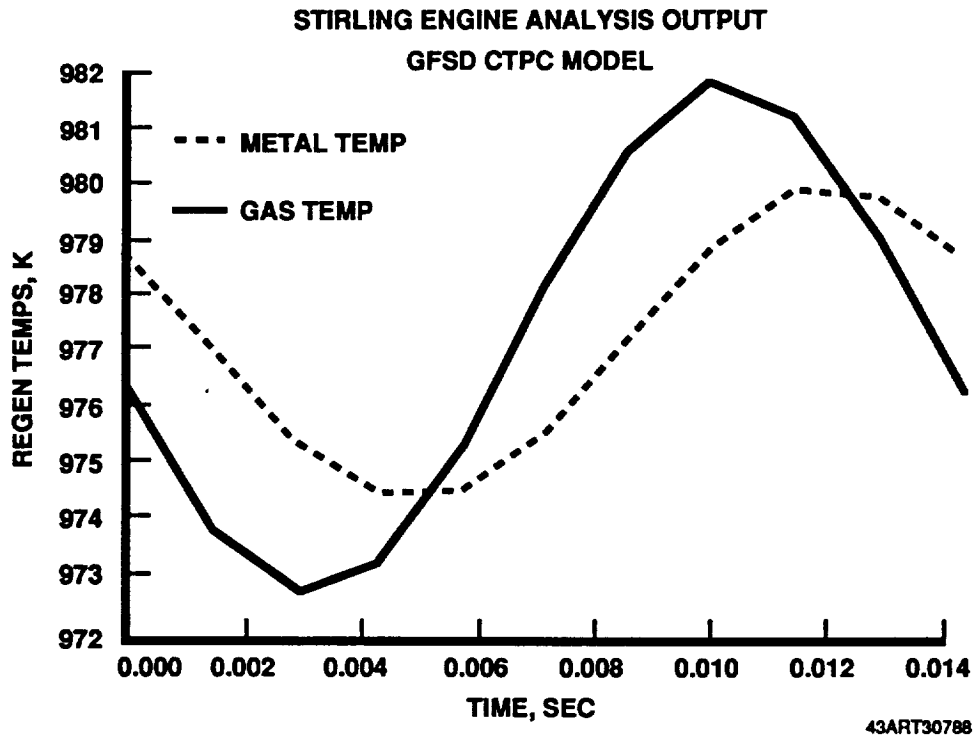

Figure 16. Regenerator Temperatures

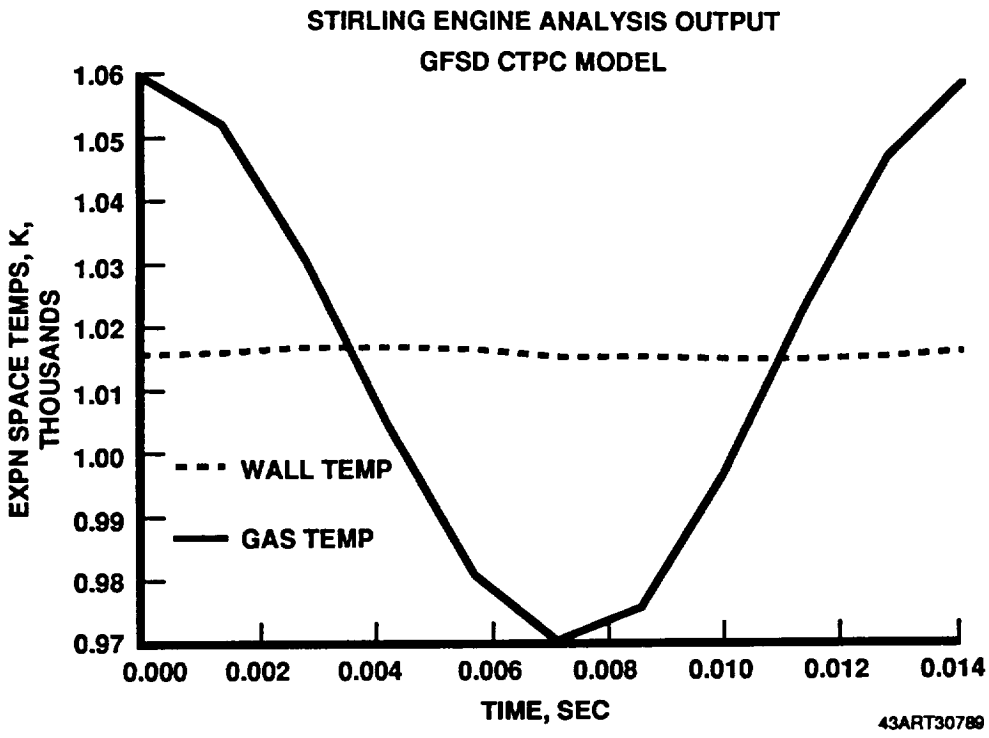

Figure 17. Expansion Space Temperatures

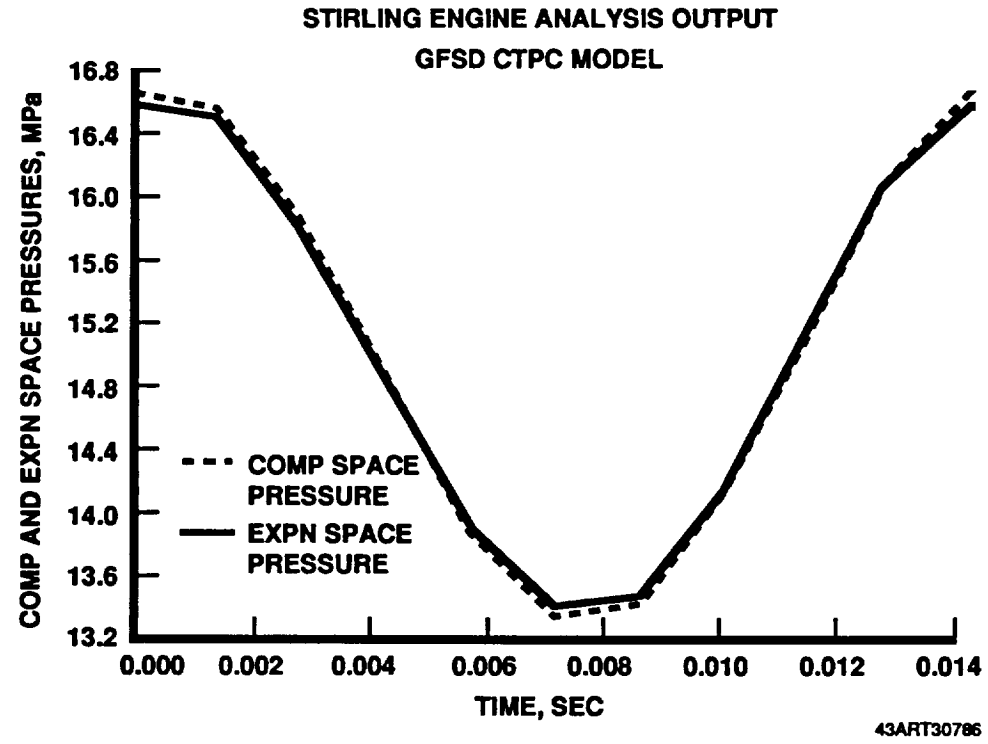

Figure 18. Compression and Expansion Space Pressures

Appendix 2. TLPDB Literature Search Titles

This appendix contains the titles of the articles found in the literature search conducted as part of the transient liquid phase diffusion bonding study. The search was performed by Nerac Inc. and the number preceding each title is a Nerac identification number. Further information on these articles can be obtained by contacting Nerac or the NASA Lewis Research Center at the following addresses:

Nerac Inc.
One Technology Drive
Toliand, CT 06084

Lanny G. Thieme MS 301-2
Stirling Technology Branch
NASA Lewis Research Center
Cleveland, OH 44135

CITATIONS FROM WELDASEARCH - THE WELDING INSTITUTE: WLD		
1.	NDN 005-0011-3221-6:	NICKEL-BASE BRAZING FILLER FOR HIGH TEMPERATURE BRAZED JOINTS (NICKELBASIS-LOT FUR HOCKTEMPERATUR-...)
2.	NDN 005-0011-3219-8	METHOD FOR MANUFACTURE OF A WORKPIECE OF DESIRED CROSS-SECTIONAL DIMENSIONS FROM AN OXIDE DISPERSION HARDENED NICKEL BASE SUPERALLOY WITH DIRECTED COARSE RADIAL CRYSTALLISATION (VERFAHREN ZUR HERSTELLUNG... STENGELKRISTALLEN)
3.	NDN 005-0011-2315-0	TRANSIENT LIQUID INSERT METAL DIFFUSION BONDING OF NICKEL-BASE SUPERALLOYS
4.	NDN 005-0011-1432-9	METHOD OF FORMING A JOINT BETWEEN A TI-AL ALLOY MEMBER AND A STEEL STRUCTURAL MEMBER
5.	NDN 005-0010-9511-6	DIFFUSION BRAZING OF NICKEL BASED SUPERALLOYS; SOME BASIC ASPECTS
6.	NDN 005-0010-9420-3	ALLOY AND METHODS OF USE THEREOF (NICKEL ALLOY BRAZING FOIL, ETC.)
7.	NDN 005-0010-9258-9	POWDER ALLOY MIX AND SUPERALLOY ARTICLE REPAIR METHOD
8.	NDN 005-0010-8982-7	THE EFFECT OF NI-CR-AL COMPOSITION ON THE DURABILITY OF ZRO2 THERMAL BARRIER COATINGS
9.	NDN 005-0010-7988-3	BEHAVIOUR OF PRECIPITATES IN NICKEL BASED SUPERALLOY, WASPALOY
10.	NDN 005-0010-6493-4	MICROSTRUCTURE AND HIGH TEMPERATURE TENSILE PROPERTIES OF BRAZED JOINTS WITH GOLD-NICKEL FILLER METAL AND AMORPHOUS NICKEL-BASE FILLER METAL
11.	NDN 005-0010-5920-3	CERIUM OXIDE STABILISED THERMAL BARRIER COATINGS
12.	NDN 005-0010-4967-2	THEORETICAL RESEARCH ON TRANSIENT LIQUID INSERT METAL DIFFUSION BONDING OF NICKEL BASE ALLOYS
13.	NDN 005-0010-0116-0	NICKEL BASE BRAZING ALLOY AND METHOD
14.	NDN 005-0009-8618-0	USE OF HIP (HOT ISOSTATIC PRESSING) TO HEAL LIQUATION CRACKS IN THE HEAT AFFECTED ZONE OF NI-BASE SUPERALLOY WELDS
15.	NDN 005-0009-8601-5	MULTIPLE FOIL TRANSIENT LIQUID PHASE BONDING
16.	NDN 005-0009-8393-2	JOINING OF NICKEL-BASED SUPERALLOYS BY LIQUID PHASE BONDING AND HOT ISOSTATIC PRESSING
17.	NDN 005-0009-7939-4	METHOD OF JOINING SUPERALLOY COMPONENTS (BY HEAT AND PRESSURE) (VERFAHREN ZUM VERBINDEN VON BAUTEILEN ...)
18.	NDN 005-0009-7188-7	WELDING THE ADVANCED ALLOYS
19.	NDN 005-0009-6389-1	INERTIA FRICTION WELDING OF SUPERALLOYS - EXPERIENCE GAINED AND FUTURE ASPECTS (SCHWUNGRADREIBSCHWEISSEN ...)
20.	NDN 005-0009-3075-7	DIFFUSION BONDING OF CAST AND EB WELDING OF PM (POWDER METALLURGY) NICKEL-BASE SUPERALLOYS
21.	NDN 005-0009-3074-5	MICROSTRUCTURAL DAMAGES INDUCED DURING THE REPAIR PROCESS
22.	NDN 005-0009-3006-0	HOMOGENEOUS ALLOY POWDER AND SUPERALLOY ARTICLE REPAIR METHOD

CITATIONS FROM WELDASEARCH - THE WELDING INSTITUTE: WLD		
23.	NDN 005-0009-2615-8	METHOD FOR JOINING TWO COMPONENT WORKPIECES MADE OF A SUPERALLOY, BY THE DIFFUSION BONDING PROCESS (VERFAHREN ZUM VERBINDEN VON TEIL-WERKSTUCKEN ...)
24.	NDN 005-0009-2329-7	HIP (HOT ISOSTATIC PRESSING) DIFFUSION BONDING OF PM (POWDER METALLURGY) ALLOYS FOR COMPOSITE LAND-BASED GAS TURBINE
25.	NDN 005-0009-0190-3	EVALUATION OF DDH (DIFFUSION DENSIFICATION HEALING) AND WELD REPAIRED F100 TURBINE VANES UNDER SIMULATED SERVICE CONDITIONS
26.	NDN 005-0009-0189-7	REPAIR TECHNIQUES FOR GAS TURBINE COMPONENTS
27.	NDN 005-0008-9329-3	THE EFFECT OF FAST NEUTRON IRRADIATION UPON THE FATIGUE-CRACK PROPAGATION BEHAVIOUR OF ALLOY 718 PLATE AND WELDMENTS
28.	NDN 005-0008-8538-7	METHOD OF BRAZING WITH NICKEL BASED ALLOY
29.	NDN 005-0008-8101-1	TLP (TRANSIENT LIQUID PHASE) WELDABILITY OF NICKEL BASE SUPERALLOYS
30.	NDN 005-0008-7086-4	STUDY ON DIFFUSION WELDING OF GAMMA-PRIME PRECIPITATION HARDENING NICKEL-BASE CAST ALLOYS. EFFECT OF SOME FACTORS ON PRECIPITATION OF GAMMA-PRIME IN LIQUID PHASE DIFFUSION WELD OF GAMMA-PRIME PRECIPITATION HARDENING NICKEL-BASE CAST ALLOYS
31.	NDN 005-0008-6498-0	NICKEL BASE BRAZING ALLOY
32.	NDN 005-0008-5487-1	SOLID STATE PRODUCTION OF MULTIPLE SINGLE CRYSTAL ARTICLES
33.	NDN 005-0008-5220-5	A CLOSED LOOP CONTROL SYSTEM FOR THREE-PHASE RESISTANCE SPOT WELDING
34.	NDN 005-0008-5059-2	DEVELOPMENT OF A NEW BRAZING TECHNIQUE FOR REPAIR OF TURBINE ENGINE COMPONENTS
35.	NDN 005-0008-4968-1	DIFFUSION WELDING OF MA 6000 AND A CONVENTIONAL NICKEL-BASE SUPERALLOY
36.	NDN 005-0008-4877-9	A CLOSED LOOP CONTROL SYSTEM FOR THREE-PHASE RESISTANCE SPOT WELDING
37.	NDN 005-0008-4716-7	DEVELOPMENT OF A NEW BRAZING TECHNIQUE FOR REPAIR OF TURBINE ENGINE COMPONENTS
38.	NDN 005-0008-4625-4	DIFFUSION WELDING OF MA 6000 AND A CONVENTIONAL NICKEL-BASE SUPERALLOY
39.	NDN 005-0008-2285-7	FLYWHEEL FRICTION WELDING OF NICKEL BASE SUPERALLOYS OF DIFFERENT HOT DUCTILITY
40.	NDN 005-0008-1412-5	SERRATED GRAIN BOUNDARY FORMATION POTENTIAL OF NI-BASED SUPERALLOYS AND ITS IMPLICATIONS
41.	NDN 005-0008-1387-0	LASER-TREATED PLASMA-SPRAYED NI-BASE ALLOY COATINGS
42.	NDN 005-0008-1345-5	THE APPLICATION OF NI-BASE FILLER MATERIALS FOR BRAZING IN AIR (APLIKACE PRASKOVYCH PRIDAVNYCH MATERIALU ...)
43.	NDN 005-0007-9917-3	MICROSTRUCTURE AND DURABILITY OF ZIRCONIA THERMAL BARRIER COATINGS (COATING, FAILURE, OXIDATION)
44.	NDN 005-0007-9405-9	NICKEL-BASED BRAZING FILLER METALS

CITATIONS FROM WELDASEARCH - THE WELDING INSTITUTE: WLD		
45.	NDN 005-0007-8472-8	TLP (TRANSIENT LIQUID PHASE) WELDABILITY OF NICKEL-BASE SUPERALLOYS
46.	NDN 005-0007-8344-0	LOW TEMPERATURE, HIGH STRENGTH NICKEL BASED BRAZING ALLOYS
47.	NDN 005-0007-6829-2	EFFECT OF HEAT TREATMENT ON THE TENSILE AND FRACTURE TOUGHNESS BEHAVIOUR OF ALLOY 718 (NICKEL BASED SUPERALLOY) WELDMENTS
48.	NDN 005-0007-6802-4	METHOD FOR PRODUCING METALLIC ARTICLES HAVING DURABLE CERAMIC THERMAL BARRIER COATINGS
49.	NDN 005-0007-6663-5	FRICTION WELDING WITH SUPERALLOYS PREPARED BY POWDER METALLURGY (REIBSCHWEISSEN VON PM-SUPERLEGIERUNGEN)
50.	NDN 005-0007-6399-3	STUDY ON ELECTRON BEAM WELDING OF DISSIMILAR MATERIALS FOR NUCLEAR PLANT. REPORT 1: EFFECT OF WELDING CONDITIONS ON WELD DEFECTS
51.	NDN 005-0007-5724-5	FORMING BRAZE-BONDED ABRASIVE TURBINE BLADE TIP
52.	NDN 005-0007-5394-0	STRUCTURAL ALLOYS (FOR CRYOGENIC APPLICATIONS)
53.	NDN 005-0007-2641-8	THE TRANSIENT LIQUID PHASE [(TLP) DIFFUSION] BONDING OF (NICKEL-BASE) SUPERALLOY K18 AND THE DIFFUSION BEHAVIOUR OF THE ELEMENT BORON
54.	NDN 005-0007-1947-5	P/M (POWDER METALLURGY) DUAL-PROPERTY WHEELS FOR SMALL ENGINES
55.	NDN 005-0007-1633-4	REPAIR TECHNIQUES FOR HOT GAS PATH COMPONENTS IN INDUSTRIAL GAS TURBINES
56.	NDN 005-0006-8614-7	FABRICATION OF GAS TURBINE NOZZLES
57.	NDN 005-0006-8412-6	TURBINE AIRFOIL REPAIR
58.	NDN 005-0006-8203-8	JOINING OF NICKEL-BASE SUPERALLOYS BY HOT ISOSTATIC PRESSING
59.	NDN 005-0006-6485-1	IMPROVING THE WELDABILITY OF NI-BASE SUPERALLOY (IN) 713C
60.	NDN 005-0006-6484-0	HIGH TEMPERATURE ELECTRON BEAM WELDING OF THE NICKEL-BASE SUPERALLOY IN-738 LC
61.	NDN 005-0006-5297-6	DIFFUSION WELDING PROCESS, APPLICATIONS, MATERIALS, AND TESTING
62.	NDN 005-0006-2903-6	REHEAT CRACKING IN NICKEL-BASE SUPERALLOYS
63.	NDN 005-0006-2201-7	THE RELATIONSHIP BETWEEN WELD HEAT-AFFECTED ZONE CRACKING AND MICROSTRUCTURE IN NICKEL-BASE SUPERALLOYS
64.	NDN 005-0006-1996-1	IN-939: A CORROSION RESISTANT ALLOY FOR INDUSTRIAL AND MARINE TURBINE BLADES
65.	NDN 005-0006-0049-6	BEHAVIOUR OF BRAZED NICKEL ALLOY UNDER CYCLIC AND THERMAL LOAD
66.	NDN 005-0005-6818-7	PROCESS AND METALLURGICAL FACTORS IN JOINING SUPERALLOYS AND OTHER HIGH SERVICE TEMPERATURE MATERIALS
67.	NDN 005-0005-5754-2	TRANSIENT LIQUID PHASE (TLP) DIFFUSION BONDING OF NICKEL-BASE HEAT RESISTING ALLOYS
68.	NDN 005-0005-1785-4	BACKER FOR ELECTRON BEAM HOLE DRILLING

CITATIONS FROM WELDASEARCH - THE WELDING INSTITUTE: WLD		
69.	NDN 005-0005-1155-4	THE MECHANISM OF DIFFUSION BRAZING OF NI-BASE SUPERALLOYS
70.	NON 005-0004-8887-8	PROCESS AND METALLURGICAL FACTORS IN JOINING SUPERALLOYS AND OTHER HIGH SERVICE TEMPERATURE MATERIALS
71.	NON 005-0004-8756-4	INTERLAYERS WITH AMORPHOUS STRUCTURE FOR BRAZING AND DIFFUSION BONDING
72.	NON 005-0004-8654-7	TRENDS IN WELDING AND JOINING TECHNOLOGY
73.	NON 005-0004-7612-8	METHOD OF (DIFFUSION) BONDING COMPOSITE TURBINE WHEELS
74.	NON 005-0004-7141-6	THE EFFECT OF PRODUCT FORM UPON FATIGUE-CRACK GROWTH BEHAVIOUR IN ALLOY 718
75.	NON 005-0004-6654-8	METHOD FOR FABRICATING COMPOSITE BLADED WHEEL ASSEMBLIES

CITATIONS FROM ENGINEERING MEETINGS (EIM): EIM		
1.	NDN 047-0061-4860-1	BRAZE REPAIR OF MA754 AERO GAS TURBINE ENGINE NOZZLES
2.	NDN 047-0055-5267-2	JOINING OF SUPERALLOYS: A SUMMARY AND EVALUATION OF WORK DONE WITHIN THE COST 50 III AND COST 501 PROGRAMS
3.	NDN 047-0055-5241-6	DIFFUSION BONDING OF CAST AND EB-WELDING OF PM NICKEL-BASE SUPERALLOYS
4.	NDN 047-0055-5240-4	MICROSTRUCTURAL DAMAGES INDUCED DURING THE REPAIR PROCESS
5.	NDN 047-0055-5229-5	ALLOY DESIGN OF SUPERALLOYS BY THE D-ELECTRONS CONCEPT
6.	NDN 047-0053-9803-8	FINITE ELEMENT THERMAL STRESS SOLUTIONS FOR THERMAL BARRIER COATINGS
7.	NDN 047-0049-6091-2	ELECTRON BEAM REFINING OF NICKEL-BASE SUPERALLOYS
8.	NDN 047-0048-7275-0	HIP DIFFUSION BONDING OF P/M ALLOYS FOR COMPOSITE LAND-BASED GAS TURBINE BUCKETS
9.	NDN 047-0048-3689-7	INERTIA FRICTION WELDING OF SUPER-ALLOYS - EXPERIENCE GAINED AND FUTURE ASPECTS
10.	NDN 047-0048-1223-6	NEW DEVELOPMENTS IN ELECTROFORMED NICKEL-BASE STRUCTURAL ALLOYS
11.	NDN 047-0046-2586-2	STRUCTURES AND REMELT TEMPERATURE OF NICKEL BASE SUPERALLOY JOINT BRAZED WITH NICKEL BASE FILLER METALS
12.	NDN 047-0045-9155-4	NOTCH TOUGHNESS AND HIGH TEMPERATURE PROPERTIES OF GOLD ALLOY AND AMORPHOUS NICKEL ALLOY BRAZED JOINTS
13.	NDN 047-0045-9145-1	IMPROVEMENT OF LIQUID PHASE DIFFUSION WELDABILITY OF INCONEL 713C BY USE OF AMORPHOUS INTERLAYERS
14.	NDN 047-0043-6665-0	ON THE ROLE OF MOLYBDENUM IN RAPIDLY SOLIDIFIED NICKEL-BASE ALLOYS
15.	NDN 047-0042-8615-0	PRECIOUS METALS - VITAL TO THE SPACE SHUTTLE OPERATION
16.	NDN 047-0035-6447-6	RAPID SOLIDIFICATION AND DYNAMIC COMPACTION OF NI-BASE SUPERALLOY POWDERS
17.	NDN 047-0028-5220-6	MICROSTRUCTURE AND DURABILITY OF ZIRCONIA THERMAL BARRIER COATINGS

CITATIONS FROM ENGINEERING MEETINGS (EIM): EIM		
18.	NDN 047-0027-3727-2	TWENTIETH ANNUAL AIRLINE PLATING AND METAL FINISHING FORUM & EXPOSITION
19.	NDN 047-0022-7190-8	HIGH TEMPERATURE VACUUM BRAZING OF THE GAS TURBINE ALLOY IN-738LC
20.	NDN 047-0021-2559-0	OXIDATION BEHAVIOR OF A THERMAL BARRIER COATING

CITATIONS FROM CA SEARCH - APPLIED: APP		
1.	NDN-044-0181-5228-0	INSERT MATERIALS AND METHOD FOR SOLID BONDING OF NICKEL-BASE SUPERALLOYS
2.	NDN-044-0169-6910-4	THERMAL BARRIER BOND COAT OBTAINED BY ELECTROPHORETIC DEPOSITION OF MCRALY POWDERS ON A NICKEL-BASED SUPERALLOY
3.	NDN-044-0165-7156-0	PROPERTIES OF A HIGH-STRENGTH, NICKEL-BASE ALLOY TUBULAR COLD-SWAGED FOR INTEGRAL JOINT CONNECTION
4.	NDN-044-0161-9949-9	JOINING OF NICKEL-BASED SUPERALLOYS BY LIQUID PHASE BONDING AND HOT ISOSTATIC PRESSING
5.	NDN-044-0159-9861-3	NICKEL BASE BRAZING ALLOY AND METHOD
6.	NDN-044-0159-0642-1	METHOD OF BONDING COLUMBIUM TO NICKEL AND NICKEL BASED ALLOYS USING LOW BONDING PRESSURES AND TEMPERATURES
7.	NDN-044-0150-6332-6	DIFFUSION BONDING OF CAST AND EB-WELDING OF PM NICKEL-BASE SUPERALLOYS
8.	NDN-044-0142-5737-0	NOTCH TOUGHNESS OF BRAZED JOINTS WITH GOLD-NICKEL FILLER METAL AND AMORPHOUS NICKEL-BASE FILLER METAL
9.	NDN-044-0139-9917-1	SURFACE PREPARATION OF NICKEL BASE ALLOYS FOR BRAZING
10.	NDN-044-0120-2700-1	MICROSTRUCTURAL INVESTIGATIONS OF A NICKEL-BASED REPAIR COATING PROCESSED BY LIQUID-PHASE DIFFUSION SINTERING
11.	NDN-044-0118-2438-0	STUDY OF BORON DIFFUSION IN HIGH-TEMPERATURE NICKEL-BASE ALLOYS BY MEANS OF SOLID-STATE TRACK DETECTORS
12.	NDN-044-0101-7351-8	JOINING OF NICKEL-BASE SUPERALLOYS BY HOT ISOSTATIC PRESSING
13.	NDN-044-0074-9279-7	THEORETICAL CONSIDERATIONS ON THE METALLURGICAL PROCESS IN T.L.P. BONDING OF NICKEL-BASE SUPERALLOYS
14.	NDN-044-0067-6623-3	STUDY ON THE MECHANISM OF DIFFUSION BRAZING OF NICKEL-BASE SUPERALLOYS
15.	NDN-044-0054-7027-0	TRANSIENT LIQUID PHASE (T.L.P.) DIFFUSION BONDING OF NICKEL-BASE HEAT RESISTING ALLOYS
16.	NDN-044-0020-0349-8	DIFFUSION BONDING NICKEL-BASE SUPERALLOYS UTILIZING A TRANSIENT LIQUID PHASE
17.	NDN-044-0007-9375-5	COMPARISON OF INERTIA BONDED AND ELECTRON BEAM WELDED JOINTS IN A NICKEL-BASE SUPERALLOY

CITATIONS FROM WORLD ALUMINIUM ABSTRACTS (WAA): WAA		
1.	NDN-034-0014-4786-1	CERAMIC COMPOSITE BODY
2.	NDN-034-0013-9858-8	DEVELOPMENT OF THERMAL BARRIER COATINGS FOR DIESEL APPLICATIONS
3.	NDN-034-0013-9014-0	NEW MATERIALS AND THEIR SUITABILITY FOR WELDING. (RETROACTIVE COVERAGE)
4.	NDN-034-0013-8976-9	CRYOGENIC STRUCTURAL MATERIALS AND THEIR WELDING AND JOINING
5.	NDN-034-0013-5983-2	DIFFUSION BONDING IN SUPERPLASTIC MATERIALS
6.	NDN-034-0012-8474-1	AIRCRAFT CORROSION PROBLEMS AND RESEARCH IN THE NETHERLANDS
7.	NDN-034-0008-8511-0	BONDING PROCESSES DURING THE DYNAMIC COMPACTION OF METALLIC POWDERS
8.	NDN-034-0005-0472-1	AN EVALUATION OF A HIGH POWER CO2 (CW) LASER AS A WELDING SOURCE

CITATIONS FROM USG/NTIS: USG		
1.	NDN 033-0129-0706-3	LANGZEITVERHALTEN WARMFESTER STAEHLE UND HOCHTEMPERATURWERKSTOFFE. (LONG-TERM BEHAVIOUR OF HIGH-TEMPERATURE STEELS AND OTHER HIGH-TEMPERATURE MATERIALS).
2.	NDN 033-0122-9112-0	THERMAL EXPANSION MISMATCH AND PLASTICITY IN THERMAL BARRIER COATING
3.	NDN 033-0121-4608-8	MICROSTRUCTURAL ASPECTS OF ZIRCONIA THERMAL BARRIER COATINGS
4.	NDN 033-0109-5308-2	CHEMISTRY OF GLASS-CERAMIC TO METAL BONDING FOR HEADER APPLICATIONS: 2. HYDROGEN BUBBLE FORMATION DURING GLASS-CERAMIC TO METAL SEALING
5.	NDN 033-0107-7851-0	FUNDAMENTAL STUDY OF THE BONDING OF THERMAL BARRIER COATINGS
6.	NDN 033-0099-7856-0	SHOCK CONSOLIDATION OF IN-100 NICKEL-BASE SUPERALLOY POWDER
7.	NDN 033-0098-4407-4	PROPERTIES AND MICROSTRUCTURES FOR DUAL ALLOY COMBINATIONS OF THREE SUPERALLOYS WITH ALLOY 901
8.	NDN 033-0095-2646-5	UNDERSTANDING THE ROLES OF THE STRATEGIC ELEMENT COBALT IN NICKEL BASE SUPERALLOYS
9.	NDN 033-0083-0673-1	APPLICATIONS OF COMPOSITE GAS-TURBINE COMPONENTS. FINAL REPORT. PHASE I
10.	NDN 033-0078-8507-3	GUIDELINES FOR THE USE OF SUPERPLASTIC FORMING OF METALS IN SPACECRAFT CONSTRUCTION
11.	NDN 033-0076-1852-6	APPLICATIONS OF COMPOSITE GAS TURBINE COMPONENTS. SEMI-ANNUAL TECHNICAL PROGRESS REPORT PHASE 1.
12.	NDN 033-0070-5563-5	APPLICATIONS OF COMPOSITE GAS TURBINE COMPONENTS. PHASE I. SEMI-ANNUAL TECHNICAL PROGRESS REPORT
13.	NDN 033-0069-7493-1	MATERIALS REVIEW FOR IMPROVED AUTOMOTIVE GAS-TURBINE ENGINE FINAL REPORT

CITATIONS FROM USG/NTIS: USG		
14.	NDN 033-0057-0444-0	INVESTIGATION OF REJUVENATION OF FATIGUE DAMAGE IN IN-718
15.	NDN 033-0039-4103-3	REVIEW OF RECENT DEVELOPMENTS: METAL JOINING
16.	NDN 033-0037-6022-1	REVIEW OF RECENT DEVELOPMENTS. POWDER METALLURGY
17.	NDN 033-0035-3257-1	DESIGN FABRICATION AND EVALUATION OF GATORIZED (TM) CERAMIC-WROUGHT ALLOY ATTACHMENT CONCEPTS
18.	NDN 033-0028-4570-0	FABRICATION OF TUNGSTEN WIRE REINFORCED NICKEL-BASE ALLOY COMPOSITES
19.	NDN 033-0025-8373-0	DEVELOP FABRICATE AND TEST HIGH STRENGTH DIRECTIONALLY SOLIDIFIED EUTECTIC ALLOYS

CITATIONS FROM NASA: NAS		
1.	NDN 020-0166-7623-3	BRAZING OF REACTION-BONDED SILICON CARBIDE AND INCONEL 600 WITH AN IRON-BASED ALLOY
2.	NDN 020-0165-9371-6	MICROSTRUCTURE AND PERFORMANCE OF NI-HF BRAZING FILLER ALLOY
3.	NDN 020-0165-0134-2	STUDIES OF CERAMIC-LIQUID METAL REACTION INTERFACES
4.	NDN 020-0164-9625-5	THE CHEMICAL COMPATIBILITY AND TENSILE BEHAVIOR OF AN NI3AL-BASED COMPOSITE
5.	NDN 020-0163-3671-9	RELATIONSHIPS BETWEEN PRIMARY MORPHOLOGY AND CRYSTAL STRUCTURE OF MC CARBIDES PRECIPITATED IN SUPERALLOYS
6.	NDN 020-0163-3095-0	EXTENDED NODES AND APB ENERGY IN A L1(2) NI-BASE SUPERALLOY
7.	NDN 020-0160-9552-2	INFLUENCE OF SECOND PHASE ON THE MECHANISM OF INTERACTION BETWEEN FATIGUE AND CREEP FOR GH33A
8.	NDN 020-0160-6997-3	THE TENSILE BEHAVIOR OF A NI3AL-BASED COMPOSITE WITH TIC REINFORCEMENT
9.	NDN 020-0157-2574-1	SKIN EFFECT OF HF-RICH MELTS AND SOME ASPECTS IN ITS USAGE FOR HF-CONTAINING CAST NICKEL-BASE SUPERALLOYS
10.	NDN 020-0156-6511-2	THERMAL BARRIER BOND COAT OBTAINED BY ELECTROPHORETIC DEPOSITION OF MCRALY POWDERS ON A NICKEL-BASED SUPERALLOY
11.	NDN 020-0155-2419-0	THERMAL EXPANSION MISMATCH AND PLASTICITY IN THERMAL BARRIER COATING
12.	NDN 020-0154-1691-4	MICROSTRUCTURAL ASPECTS OF ZIRCONIA THERMAL BARRIER COATINGS
13.	NDN 020-0152-8724-5	CERIUM OXIDE STABILIZED THERMAL BARRIER COATINGS
14.	NDN 020-0146-0429-2	JOINING OF SUPERALLOYS - A SUMMARY AND EVALUATION OF WORK DONE WITHIN THE COST 50 III AND COST 501 PROGRAMS
15.	NDN 020-0146-0409-7	DIFFUSION BONDING OF CAST AND EB-WELDING OF PM NICKEL-BASE SUPERALLOYS
16.	NDN 020-0146-0399-8	ALLOY DESIGN OF SUPERALLOYS BY THE D-ELECTRONS CONCEPT
17.	NDN 020-0145-9941-1	THE EFFECT OF NICRAL COMPOSITION ON THE DURABILITY OF THE ZR02 THERMAL BARRIER COATINGS

CITATIONS FROM NASA: NAS		
18.	NDN 020-0144-4299-1	PREPARATION AND CHARACTERIZATION OF GAMMA(NI)/GAMMA-PRIME(N-I3AL) SYNTHETIC-PHASE JOINTS
19.	NDN 020-0143-7428-6	CHEMISTRY OF GLASS-CERAMIC TO METAL BONDING FOR HEADER APPLICATIONS PART 2: HYDROGEN BUBBLE FORMATION DURING GLASS-CERAMIC TO METAL SEALING
20.	NDN 020-0135-5829-8	THE BNI-5 - INCONEL 718 'BINARY' SYSTEM
21.	NDN 020-0134-6753-0	SHOCK CONSOLIDATION OF IN-100 NICKEL-BASE SUPERALLOY POWDER
22.	NDN 020-0134-0692-9	DIFFUSION WELDING OF MA 6000 AND A CONVENTIONAL NICKEL-BASE SUPERALLOY
23.	NDN 020-0133-3940-0	PRECIPITATION AROUND WELDS IN THE NICKEL-BASE SUPERALLOY. INCONEL 718
24.	NDN 020-0133-2310-6	DISPERSION STRENGTHENED NICKEL FOR GAS TURBINE APPLICATIONS
25.	NDN 020-0131-6936-1	RAPID SOLIDIFICATION AND DYNAMIC COMPACTION OF NI-BASE SUPERALLOY POWDERS
26.	NDN 020-0130-0432-3	EFFECT OF HEAT-TREATMENT UPON THE FATIGUE-CRACK GROWTH BEHAVIOR OF ALLOY 718 WELDMENTS. I - MACROSCOPIC BEHAVIOR II - MICROSCOPIC BEHAVIOR
27.	NDN 020-0127-8565-9	UNDERSTANDING THE ROLES OF THE STRATEGIC ELEMENT COBALT IN NICKEL BASE SUPERALLOYS
28.	NDN 020-024-7243-8	EFFECT OF MG CONTENT ON CREEP BEHAVIOUR OF NI-BASE WROUGHT SUPERALLOY
29.	NDN 020-0119-7683-4	APPLICATIONS OF COMPOSITE GAS-TURBINE COMPONENTS. PHASE 1 FINAL REPORT
30.	NDN 020-0117-2835-8	HIGH TEMPERATURE ALLOYS FOR GAS TURBINES 1982; PROCEEDINGS OF THE CONFERENCE, LIEGE, BELGIUM, OCTOBER 4-6, 1982
31.	NDN 020-0117-2790-1	BLADE REPAIR AND RECOVERY
32.	NDN 020-0115-1795-5	CAUSES OF FRACTURE BEHAVIOR IN VIBRATIONALLY LOADED HIGH-TEMPERATURE SOLDERED JOINTS
33.	NDN 020-0114-3551-3	GUIDELINES FOR THE USE OF SUPERPLASTIC FORMING OF METALS IN SPACECRAFT CONSTRUCTION
34.	NDN 020-0113-6909-7	DEVELOPMENT OF HYBRID GAS TURBINE BUCKET TECHNOLOGY
35.	NDN 020-0113-3713-8	APPLICATIONS OF COMPOSITE GAS TURBINE COMPONENTS SEMIANNUAL TECHNICAL PROGRESS REPORT
36.	NDN 020-0112-6957-1	THE DEVELOPMENT OF GAS TURBINE MATERIALS
37.	NDN 020-0096-9480-8	THERMAL JOINING OF HIGH TEMPERATURE RESISTANT CASTING MATERIALS
38.	NDN 020-0094-7369-5	INVESTIGATION OF REJUVENATION OF FATIGUE DAMAGE IN IN-718 FINAL REPORT, 1 JAN. 1976 - 31 JAN. 1978
39.	NDN 020-0092-4590-0	HOT-CORROSION-RESISTANT DUPLEX COATINGS FOR A SUPERALLOY
40.	NDN 020-0091-2709-4	TURBINE AIRFOIL REPAIR
41.	NDN 020-0089-7772-0	NEAR-NET-SHAPE ENGINE METHODS EMERGE

CITATIONS FROM NASA: NAS		
42.	NDN 020-0089-0812-6	BEHAVIOR OF BRAZED NICKEL ALLOY UNDER CYCLIC AND THERMAL LOAD
43.	NDN 020-0082-7786-2	PROCESS AND METALLURGICAL FACTORS IN JOINING SUPERALLOYS AND OTHER HIGH SERVICE TEMPERATURE MATERIALS
44.	NDN 020-0079-8147-8	SOME ION PROBE MASS SPECTROMETER OBSERVATIONS OF NICKEL ACTIVATED RECRYSTALLIZATION OF DOPED TUNGSTEN AND TZM
45.	NDN 020-0076-3515-1	DESIGN, FABRICATION, AND EVALUATION OF GATORIZED(TM) CERAMIC-WROUGHT ALLOY ATTACHMENT CONCEPTS STATUS REPORT. 1 JUL. 1974 - 31 DEC. 1975
46.	NDN 020-0072-9154-1	HIGH TEMPERATURE CREEP IN A SEMI-COHERENT NIAL-NI2ALTI ALLOY
47.	NDN 020-0067-1807-3	FABRICATION OF TUNGSTEN WIRE REINFORCED NICKEL-BASE ALLOY COMPOSITES
48.	NDN 020-0063-0564-7	HIGH-TEMPERATURE BRAZING
49.	NDN 020-0059-3822-3	DIFFUSION BONDING AND ITS APPLICATION TO MANUFACTURING
50.	NDN 020-0052-3147-4	METHODS FOR DIFFUSION WELDING THE SUPERALLOY UDIMET 700

CITATIONS FROM MECHANICAL ENGINEERING (ISMEC): ISM		
1.	NDN 016-0016-2507-4	MICROSTRUCTURAL INVESTIGATIONS OF A NICKEL-BASED REPAIR COATING PROCESSED BY LIQUID PHASE DIFFUSION SINTERING
2.	NDN 016-0014-4430-4	USE OF ELECTRODEPOSITION TO PROVIDE COATINGS FOR SOLID STATE BONDING
3.	NDN 016-0013-0944-9	SOME MICROSTRUCTURAL FEATURES OF NI-AL-MO-BASE SUPERALLOYS

CITATIONS FROM ENGINEERING INDEX: EIX		
1.	NDN 007-0208-2117-0	TRANSIENT LIQUID PHASE BONDING FOR MARM-247 AND IN939
2.	NDN 007-0208-0013-0	ELECTRONIC STRUCTURE OF $GAMMA$ $PRIME$ PHASE CONTAINING ZR IN NICKEL-BASE SUPERALLOY
3.	NDN 007-0205-7761-1	CHEMICAL COMPATIBILITY AND TENSILE BEHAVIOR OF AN NI/3AL-BASED COMPOSITE
4.	NDN 007-0203-0041-8	STUDIES OF CERAMIC-LIQUID METAL REACTION INTERFACES
5.	NDN 007-0201-8603-8	INTERACTION OF REACTION-BONDED SILICON CARBIDE AND INCONEL 600 WITH A NICKEL-BASED BRAZING ALLOY
6.	NDN 007-0196-6464-7	METALLURGICAL STUDY OF TLIM BONDING. STUDY ON TRANSIENT LIQUID INSERT METAL DIFFUSION BONDING OF NI BASE SUPERALLOYS (PART 3)
7.	NDN 007-0196-6457-0	EFFECTS OF SOLID PHASE DIFFUSION WELDING CONDITION AND CARBON CONTENT OF AN INSERT METAL ON JOINT STRENGTH FOR NI-BASE SUPERALLOYS
8.	NDN 007-0196-0761-5	ANALYSIS OF ISOTHERMAL SOLIDIFICATION PROCESS ON TRANSIENT LIQUID INSERT METAL DIFFUSION BONDING. STUDY ON TRANSIENT LIQUID INSERT METAL DIFFUSION BONDING OF NI-BASE SUPERALLOYS (PART 2)

CITATIONS FROM ENGINEERING INDEX: EIX		
9.	NDN 007-0180-2322-1	SMOOTHING INTERMETALLICS BRITTLE EDGE
10.	NDN 007-0179-3206-7	JOINING OF NICKEL-BASED SUPERALLOYS BY LIQUID PHASE BONDING AND HOT ISOSTATIC PRESSING
11.	NDN 007-0176-9522-7	FINITE ELEMENT THERMAL STRESS SOLUTIONS FOR THERMAL BARRIER COATINGS
12.	NDN 007-0164-9767-7	NEW DEVELOPMENTS IN ELECTROFORMED NICKEL-BASED STRUCTURAL ALLOYS
13.	NDN 007-0161-0265-8	HIP DIFFUSION BONDING OF PM ALLOYS FOR COMPOSITE LAND-BASED GAS TURBINE BUCKETS
14.	NDN 007-0159-8686-3	LIQUID PHASE DIFFUSION BONDING OF A NICKEL-BASE OXIDE DISPERSION STRENGTHENED ALLOY MA 754
15.	NDN 007-0151-9650-4	EXAMINATION OF THE TITANIUM ENVIRONMENT IN A RENE 41 NICKEL BASE SUPERALLOY BY X-RAY ABSORPTION SPECTROSCOPY
16.	NDN 007-0150-8085-0	NOTCH TOUGHNESS OF BRAZED JOINTS WITH GOLD-NICKEL FILLER METAL AND AMORPHOUS NICKEL-BASE FILLER METAL
17.	NDN 007-0149-3206-8	BEHAVIOR OF PRECIPITATES IN NI-BASE SUPERALLOY, WASPALOY
18.	NDN 007-0149-3196-9	STUDY ON FORMATION OF ALLOYED LAYER OF LOW MELTING TEMPERATURE ON BONDING SURFACE OF IN738LC WITH SPUTTERING: STUDY ON DIFFUSION WELDING USING ALLOYED LAYER ON BONDING SURFACE (REPORT 3)
19.	NDN 007-0146-1201-3	MICROSTRUCTURE AND HIGH TEMPERATURE TENSILE PROPERTIES OF BRAZED JOINTS WITH GOLD-NICKEL FILLER METAL AND AMORPHOUS NICKEL-BASE FILLER METAL
20.	NDN 007-0146-1200-1	MICROSTRUCTURE AND HIGH TEMPERATURE TENSILE PROPERTIES OF BRAZED JOINTS WITH GOLD-NICKEL FILLER METAL AND AMORPHOUS NICKEL-BASE FILLER METAL
21.	NDN 007-0143-2361-1	DIFFUSION WELDING OF MA 6000 AND A CONVENTIONAL NICKEL-BASE SUPERALLOY
22.	NDN 007-0141-7570-1	STRENGTH AND STABILITY OF SUPERALLOYS
23.	NDN 007-0137-6513-2	TWENTIETH ANNUAL AIRLINE PLATING AND METAL FINISHING FORUM & EXPOSITION
24.	NDN 007-0127-5092-3	ALLOYING EFFECT ON THE ELECTRONIC STRUCTURE OF NI/3AL ($GAMMA$ $PRIME$)
25.	NDN 007-0125-5147-1	EFFECT OF MG CONTENT ON THE CREEP BEHAVIOR OF A NI-BASE WROUGHT SUPERALLOY
26.	NDN 007-0124-9602-2	VDM'S UNIQUE COLD-ROLL MILL FOR NICKEL GOES ON-STREAM
27.	NDN 007-0123-6082-3	GAS ATOMISATION OF HIGH TEMPERATURE ALLOY POWDERS
28.	NDN 007-0114-2024-1	HARDFACING CLOTH BYPASSES THE SPRAY OR WELD ROUTE
29.	NDN 007-0110-7201-9	USE OF ELECTRODEPOSITION TO PROVIDE COATINGS FOR SOLID STATE BONDING
30.	NDN 007-0109-6756-8	BEEINFLUSSUNG DER MECHANISCH-THERMISCHEN FESTIGKEIT VON SCHWUNGRADREIBSCHWEISSUNGEN AN WASPALOY DURCH GEZIELTE EINSTELLUNG VON GEFUGE UND STRUKTOR. (CONTROL OF THE THERMO-MECHANICAL STRENGTH OF FRICTION WELDED FLYWHEEN JOINTS IN WASPALOY BY PINPOINTED STRUCTURAL MODIFICATIONS)

CITATIONS FROM ENGINEERING INDEX: EIX		
31.	NDN 007-0108-5179-7	ZERSPANUNGSVERSUCHE ZUM TIEFSCHLEIFEN VON SONDERLEGIERUNGEN (MACHINING TESTS FOR ABRASIVE MACHINING OF SPECIAL ALLOYS)
32.	NDN 007-0105-1683-2	SOME MICROSTRUCTURAL FEATURES OF NI-AL-MO-BASE SUPERALLOYS
33.	NDN 007-0090-4832-0	LARGE DELTA WINGS FOR EARTH-TO-ORBIT TRANSPORTS
34.	NDN 007-0085-0872-4	ABLAUF DER VERBINDUNGSBILDUNG BEIM SCHWUNGRADREIBSCHWEISSEN VON HOCHWARMFESTEN LEGIERUNGEN $EM DASH$ TEMPERATURVERLAUF UND WULSTBILDUNG (DEVELOPMENT OF WELD JOINT DURING FRICTION WELDING OF SUPERALLOYS $EM DASH$ HEATING RATES AND FORMATID OF SEAM)
35.	NDN 007-0078-0842-6	ADVANCED FABRICATION PROCESSES
36.	NDN 007-0076-9767-7	THEORETICAL CONSIDERATIONS ON THE METALLURGICAL PROCESS IN T. L. P. BONDING OF NICKEL-BASE SUPERALLOYS
37.	NDN 007-0074-3128-8	BRAZING OF HASTELLOY X WITH WIDE CLEARANCE BUTT JOINTS
38.	NDN 007-0062-6706-7	PROCESS AND METALLURGICAL FACTORS IN JOINING SUPERALLOYS AND OTHER HIGH SERVICE TEMPERATURE MATERIALS
39.	NDN 007-0062-0856-7	TRANSIENT LIQUID PHASE (T. L. P.) DIFFUSION BONDING OF NICKEL-BASE HEAT RESISTING ALLOYS
40.	NDN 007-0055-5929-0	DAS VERFORMUNGSVERMOEGEN VON LOETVERBINDUNGEN MIT HOCHTEMPERATURLOTEN (FORMABILITY OF BRAZED ASSEMBLIES MADE WITH HIGH TEMPERATURE BRAZING ALLOYS)
41.	NDN 007-0050-6242-5	GEFUEGEAUFBAU DREIER NICKELBASISLOTE UND DER DAMIT HERGESTELLTEN VERBINDUGEN AN DREI HOCHWARMFESTEN WERKSTOFFEN (MICROSTRUCTURE OF THREE NICEL BASE BRAZING ALLOYS AND OF THE JOINTS PRODUCED IN THREE HIGH TEMPERATURE RESISTING MATERIALS)
42.	NDN 007-0041-5208-0	MECHANISMS TO CONTROL CREEP RESISTANCE
43.	NDN 007-0040-2924-4	ADVANCES IN METALS PROCESSING VIA FORGING
44.	NDN 007-0032-2593-1	HIGH TEMPERATURE PROPERTIES OF THE UNIDIRECTIONALLY SOLIDIFIED NI/3AL-NI//3TA EUTECTIC
4.5	NDN 007-0030-0788-5	TLP BONDING: A NEW METHOD FOR JOINING HEAT RESISTANT ALLOYS
46.	NDN 007-0024-6317-2	REPAIR OF TURBINE BLADES AND VANES
47.	NDN 007-0024-0070-8	HEAT-TREATMENT ASPECTS OF METAL-JOINING PROCESSES. PROCEEDINGS OF THE BIENNIAL CONFERENCE, LONGON, ENGL. DEC 8-9 1971, ORGANIZED BY TH HEAT TREATMENT JOINT COMMITTEE OF THE IRON AND STEEL INSTITUTE
48.	NDN 007-0017-0884-7	METHODS FOR DIFFUSION WELDING THE SUPERALLOY UDIMET 700
49.	NDN 007-006-7900-1	ACTIVATED DIFFUSION BONDING
50.	NDN 007-0003-0463-7	COMPARISON OF INERTIA BONDED AND ELECTRON BEAM WELDED JOINTS IN A NICKELL-BASE SUPERALLOY
51.	NDN 007-0001-1204-9	DIFFUSION BONDING OF SUPERALLOYS

CITATIONS FROM METALS ABSTRACTS (ASM): ASM		
1.	NDN 002-0083-5203-1	BRAZING OF REACTION-BONDED SILICON CARBIDE AND INCONEL 600 WITH AN IRON-BASED ALLOY
2.	NDN 002-0083-5030-7	DIFFUSION BONDING OF SI SUB 3 N SUB 4 TO ODS-SUPERALLOY MA-6000 BY HOT ISOSTATIC PRESSING
3.	NDN 002-0083-3980-4	EXTENDED NODES AND APB ENERGY IN A LI SUM 2 NICKEL-BASE SUPERALLOY
4.	NDN 002-0083-1807-2	HIGH TEMPERATURE METAL ALLOY MIXTURES FOR FILLING HOLES AND REPAIRING DAMAGES IN SUPERALLOY BODIES
5.	NDN 002-0082-5415-0	PRELIMINARY STUDY ON PRESSURE BRAZING AND DIFFUSION WELDING OF NB--1ZR TO INCONEL 718
6.	NDN 002-0082-4755-7	THE CHEMICAL COMPATIBILITY AND TENSILE BEHAVIOR OF AN NI SUB 3 A1-BASED COMPOSITE
7.	NDN 002-0082-0389-0	RESIDUAL STRESSES GENERATED BY ROLLING OF A TUBE INTO A PLATE (RETROACTIVE COVERAGE)
8.	NDN 002-0081-9665-3	INVESTIGATIONS OF ID STRESS CORROSION CRACKING IN FIELD AND LABORATORY PROGRAMS (RETROACTIVE COVERAGE)
9.	NDN 002-0081-9653-7	IMPROVEMENT OF THE CORROSION RESISTANCE UNDER STRESS OF STEAM GENERATOR TUBING (RETROACTIVE COVERAGE)
10.	NDN 002-0081-8869-3	STUDIES OF CERAMIC/LIQUID METAL REACTION INTERFACES
11.	NDN 002-0081-8613-1	NICKEL-BASE SOLDER FOR HIGH-TEMPERATURE SOLDER JOINTS
12.	NDN 002-0081-8491-2	VACUUM ARC BRAZING WITH POWDERED SOLDER
13.	NDN 002-0081-8273-3	EFFECTS OF BOND COAT PRE-ALUMINIZING TREATMENT ON THE PROPERTIES OF ZRO SUB 1 --8 WT.% Y SUB 2 O SUB 3 /CO--29CR--6A1--1Y THERMAL BARRIER COATINGS
14.	NDN 002-0081-8121-2	INTERFACE STABILITY IN THE NI--CR--A1 SYSTEM. II. MORPHOLOGICAL STABILITY OF BETA -NI50A1 VS. GAMMA -Ni40CR DIFFUSION COUPLE INTERFACES AT 1150 DEG C
15.	NDN 002-0081-7944-8	THE TENSILE BEHAVIOR OF A NI SUB 3 A1-BASED COMPOSITE WITH TIC REINFORCEMENT
16.	NDN 002-0081-5831-7	STRESS CORROSION CRACKING BEHAVIOR OF ALLOYS 718 AND A286
17.	NDN 002-0081-4960-2	PRODUCTION OF NEW MATERIALS BY HIP PROCESS
18.	NDN 002-0081-4900-6	LIQUID FILM MIGRATION (LFM) IN THE WELD HEAT AFFECTED ZONE (HAZ) OF A NICKEL-BASE SUPERALLOY
19.	NDN 002-0081-4824-5	THE DEPOSITION OF HARDFACING AND CORROSION RESISTANT MATERIALS BY FRICTION SURFACING
20.	NDN 002-0081-3831-8	ELECTRONIC STRUCTURE OF GAMMA ' PHASE CONTAINING ZIRCONIUM IN NICKEL-BASE SUPERALLOY
21.	NDN 002-0081-3163-4	MOLECULAR DYNAMICS SIMULATION OF THE ROLE OF GRAIN BOUNDARY CHEMISTRY ON INTERGRANULAR FRACTURE
22.	NDN 002-0081-1643-8	THE JOINING OF REACTION-BONDED SILICON CARBIDE TO INCONEL 600 USING REFRACTORY METAL INTERLAYERS
23.	NDN 002-0081-1633-5	LASER WELDING OF SLEEVES FOR NUCLEAR REACTOR PLANT HEAT EXCHANGER TUBES

CITATIONS FROM METALS ABSTRACTS (ASM): ASM		
24.	NDN 002-0081-1627-0	PROGRESS IN WELDING STUDIES FOR CANADIAN NUCLEAR FUEL WASTE DISPOSAL CONTAINERS
25.	NDN 002-0081-1463-6	HEAT TREATMENT FOR DUAL ALLOY TURBINE WHEELS
26.	NDN 002-0080-7810-3	THE ULTRASONIC WELDING PROCESS. II.
27.	NDN 002-0080-7408-0	THE OXIDE PEGGING SPALLING MECHANISM AND SPALLING MODES OF ZR0 SUB 2 8 WT.% Y SUB 2 0 SUB 3 /NI--22CR--10A1--1Y THERMAL BARRIER COATINGS UNDER VARIOUS OPERATING CONDITIONS
28.	NDN 002-0080-7185-6	THERMAL BARRIER COATING OF INCOLOY ALLOY 909
29.	NDN 002-0080-6937-0	THERMAL--MECHANICAL FATIGUE TEST APPARATUS FOR METAL MATRIX COMPOSITES AND JOINT ATTACHMENTS
30.	NDN 002-0080-6217-0	MORPHOLOGY OF WELD HEAT-AFFECTED ZONE LIQUATION CRACKING IN TANTALUM-MODIFIED CAST ALLOY 718
31.	NDN 002-0080-4556-0	METHOD FOR PRODUCTION OF A COMPOUND GAS TURBINE BLADE CONSISTING OF A FOOT, BLADE AND HEAD PIECE, WHEREBY THE BLADE IS MADE FROM A DISPERSION HARDENED NICKEL BASED SUPERALLOY; AND COMPOUND BLADE PRODUCED USING THIS METHOD
32.	NDN 002-0080-3865-8	WELDABILITY OF NICKEL-BASE SUPERALLOY GH536 SHEET
33.	NDN 002-0080-3654-6	THERMAL BARRIER COATINGS: MICROSTRUCTURAL INVESTIGATION AFTER ANNEALING
34.	NDN 002-0080-3588-8	EFFECT OF THERMAL CYCLING ON THE MICROSTRUCTURE OF CERIA-STABILIZED ZIRCONIA THERMAL BARRIER COATINGS
35.	NDN 002-0080-3583-9	THERMAL MODELLING OF VARIOUS THERMAL BARRIER COATINGS IN A HIGH HEAT FLUX ROCKET ENGINE (REPORT)
36.	NDN 002-0080-3488-4	THERMAL BARRIER COATINGS FOR GAS TURBINE USE
37.	NDN 002-0080-3354-5	OXIDATION- AND HOT CORROSION-RESISTANT NICKEL-BASE ALLOY COATINGS AND CLADDINGS FOR INDUSTRIAL AND MARINE GAS TURBINE HOT SECTION COMPONENTS AND RESULTING COMPOSITE ARTICLES
38.	NDN 002-0080-1731-0	COMPARATIVE HOT CORROSION STUDIES OF PVD (PHYSICAL VAPOUR DEPOSITED), AIR AND VACUUM PLASMA SPRAYED COATINGS
39.	NDN 002-0080-0529-0	ISSUES IN CERAMIC-TO-METAL JOINING: AN INVESTIGATION OF BRAZING A SILICON NITRIDE-BASED CERAMIC TO A LOW-EXPANSION SUPERALLOY
40.	NDN 002-0080-0432-6	AN INVESTIGATION OF INTERFACIAL MICROSTRUCTURE AND BONDING IN BRAZED SILICON NITRIDE--SILICON NITRIDE AND SILICON NITRIDE--NI--CR--FE ALLOY 600 JOINTS
41.	NDN 002-0080-0395-4	FABRICATION OF DUAL ALLOY INTEGRALLY BLADED ROTORS
42.	NDN 002-0080-0192-1	BONDING GLASS CERAMICS TO HIGH TEMPERATURE ALLOYS
43.	NDN 002-0079-7881-7	COMPOSITE ALLOY INGOT FOR USE IN INVESTMENT CASTING
44.	NDN 002-0079-7086-7	BRAZE REPAIR OF MA754 AERO GAS TURBINE ENGINE NOZZLES
45.	NDN 002-0079-7069-7	SEALING OF ALUMINUM-CONTAINING STAINLESS STEEL TO LITHIA--ALUMINA--SILICA GLASS-CERAMIC
46.	NDN 002-0079-6970-1	EFFECT OF CAST-TO-CAST VARIATIONS ON THE QUALITY OF THIN SECTION NICKEL ALLOY WELDED JOINTS (RESEARCH REPORT)

CITATIONS FROM METALS ABSTRACTS (ASM): ASM		
47.	NDN 002-0079-6727-3	BURNER RIG EVALUATION OF CERAMIC COATINGS WITH VANADIUM-CONTAMINATED FUELS
48.	NDN 002-0079-6602-5	BONDS COAT DEVELOPMENT FOR THERMAL BARRIER COATINGS
49.	NDN 002-0079-5291-9	THE ROLE OF INTERFACIAL DISLOCATION NETWORKS IN HIGH TEMPERATURE CREEP OF SUPERALLOYS
50.	NDN 002-0079-3493-0	DISSIMILAR STAINLESS HIGH-ALLOY STEEL WELDING (WITH STAINLESS AUSTENITIC STEEL OR STABILIZED FERRITIC ADDITIONS)
51.	NDN 002-0079-3480-2	THE MECHANICS OF METAL--CERAMIC BRAZING
52.	NDN 002-0079-3405-0	TRANSIENT LIQUID INSERT METAL DIFFUSION BONDING OF NICKEL BASE SUPERALLOYS. III. METALLURGICAL STUDY OF TLIM BONDING.
53.	NDN 002-0079-3399-8	EFFECTS OF SOLID PHASE DIFFUSION WELDING CONDITION AND CARBON CONTENT OF AN INSERT METAL ON JOINT STRENGTH FOR NICKEL BASE SUPERALLOYS
54.	NDN 002-0079-3389-5	ANALYSIS OF ISOTHERMAL SOLIDIFICATION PROCESS OF TRANSIENT LIQUID INSERT METAL DIFFUSION BONDING. II. STUDY ON TRANSIENT LIQUID INSERT METAL DIFFUSION BONDING OF NICKEL BASE SUPERALLOYS
55.	NDN 002-0079-3254-4	CONTROL AND DOCUMENTATION IN VACUUM FURNACE PROCESSING OF AEROSPACE METALS
56.	NDN 002-0079-3164-3	FAILURE PROCESSES WITHIN CERAMIC COATINGS AT HIGH TEMPERATURES
57.	NDN 002-0079-0260-6	ABRADABLE ARTICLE AND POWDER AND METHOD FOR MAKING
58.	NDN 002-0079-0226-6	ENDURANCE OF SCREWS IN LIGHT-GAUGE STRUCTURES
59.	NDN 002-0079-0214-0	NEW MATERIALS AND THEIR SUITABILITY FOR WELDING (RETROACTIVE COVERAGE)
60.	NDN 002-0079-0157-2	CHARACTERISTICS OF THE FRICTION WELDING PROCESS
61.	NDN 002-0079-0133-0	NEW APPLICATIONS FOR RAPIDLY SOLIDIFIED BRAZING FOILS
62.	NDN 002-0078-9853-6	DEVELOPMENT OF THERMAL BARRIER COATINGS FOR DIESEL APPLICATIONS
63.	NDN 002-0078-9802-0	SPRAY AUTOMATED BALANCING OF ROTORS: CONCEPT AND INITIAL FEASIBILITY STUDY
64.	NDN 002-0078-9662-0	FRICTION SURFACING (RETROACTIVE COVERAGE)
65.	NDN 002-0078-8841-5	INTERFACIAL SPRING MODEL FOR ULTRASONIC INTERACTIONS WITH IMPERFECT INTERFACES: THEORY OF OBLIQUE INCIDENCE AND APPLICATION TO DIFFUSION-BONDED BUTT JOINTS
66.	NDN 002-0078-7349-7	THE EUROPEAN HERITAGE AND PROGRESS IN ADVANCED MATERIALS AND PROCESSING
67.	NDN 002-006984-6	CERMETS TACKLE TOUGH JOBS
68.	NDN 002-0078-6772-2	FABRICATION TECHNOLOGIES AND PROPERTIES OF P/M SUPERALLOYS AND TITANIUM ALLOYS
69.	NDN 002-0078-6673-0	CHEMICAL MICROHETEROGENEITY OF WELDED JOINTS IN CREEP-RESISTING STEELS AND ALLOYS IN ARGON-ARC WELDING WITH FORCED COOLING (TRANSLATION)

CITATIONS FROM METALS ABSTRACTS (ASM): ASM		
70.	NDN 002-0078-6641-9	THEORETICAL RESEARCH ON TRANSIENT LIQUID INSERT METAL DIFFUSION BONDING OF NICKEL BASE ALLOYS
71.	NDN 002-0078-6625-0	ELECTRON BEAM WELDING OF THICK-WALL PRODUCTS MADE FROM HEAT RESISTANT STEEL AND ALLOYS
72.	NDN 002-0078-6561-0	REMOVAL OF HIGH TEMPERATURE BRAZING ALLOYS
73.	NDN 002-0078-6460-5	STUDY ON TRANSIENT LIQUID INSERT METAL DIFFUSION BONDING OF NICKEL-BASE SUPERALLOYS. I. DISSOLUTION PHENOMENON OF BASE METAL INTO LIQUID INSERT METAL
74.	NDN 002-0078-6401-0	COMPARISON OF ELEMENT DIFFUSIVITY IN PLASMA COATINGS AND DIFFUSION BONDS
75.	NDN 002-0078-6395-9	CRYOGENIC STRUCTURAL MATERIALS AND THEIR WELDING AND JOINING

8. REFERENCES

8.1 TLPDB Document References and Background Titles

Report References

1. Dudenhoefer, James E. and Winter, Jerry M.; "Status of NASA's Stirling Space Power Converter Program"; NASA TM 104512; Proceedings of 26th IECEC (1991); vol. 2, pp. 38-43

2. Tew, Roy C., Thieme, Lanny G., and Dudenhoefer, James E.; "Recent Stirling Engine Loss Understanding Results"; NASA TM 103122; Proceedings of 25th IECEC (1990); vol. 5, pp. 377-385

3. Jones, D.; "Space Power Free-Piston Stirling Engine Scaling Study"; NASA CR-182218; October, 1989.

4. ASM Handbook; vol. 6, 1981

5. Sims, Chester; The Superalloys; Wiley; 1972

6. Doyle, J.; Vozzella, P.; Wallace, F.; and Dunthorne, H.; "Comparison of Inertia Bonded and Electron Beam Weld Joints in a Nickel-base Superalloy;" Welding Research; November, 1969

7. Krueger, D. D.; "The Development of Direct Age 718 for Gas Turbine Disk Applications;" Proceedings of the International Symposium on the Metallurgy and Applications of Superalloy 718; 1989

8. Duvall, D.; Owczarski, W.; and Paulonis, D.; "TLP Bonding: A New Method for Joining Heat Resistant Alloys;" Welding Journal; April, 1974

9. Duvall, D.; Owczarski, W.; Paulonis, D.; and King, W.; "Methods for Diffusion Welding the Superalloy Udimet 700;" WRS; February, 1972

10. Ikawa, H,: Nakao, Y.; and Isai, T.; "Transient Liquid Insert Metal Diffusion Bonding of Nickel-base Superalloys;"

11. Ikawa, H.; Nakao, Y.; and Isai, T.; "Theoretical Considerations on the Metallurgical Process in TLP Bond of Nickel-base Superalloys;" Transactions of the J.W.S., Volume 10, Number 1; April, 1979

Liquid metal compatibility study references

12. Liquid Metals Handbook; AEC, Department of the Navy; Washington DC; 1952

13. Liquid Metals Handbook, Sodium-NaK Supplement, 1955

14. Copra, O.K.; Wang, J.Y.N; and Natesan, K.; "Review of Sodium Effects on Candidate Materials for Central Receiver Solar-Thermal Power Systems"; ANL 79-36; 1979

15. Cowgill, M.G.; "Sodium Corrosion of Alloy 718 at 649 C"; WAESD-NA-94000-16; 1984

16. Dunn, W.E.; Bonilla, C.F.; Ferstenberg, C.; and Gross, B.; "Mass Transfer in Liquid Metals"; AIChE Journal; 1956

17. Gill, W.N.; Vanek, R.P.; Jelinek, R.V.; and Grove Jr, C.S.; "Mass Transfer in Liquid-Lithium Systems"; AIChE Journal; 1960

18. Jacobson, D.L.; and Soundararajan, P.; "Failure Analysis of a Sodium Heat Pipe with Integral Lithium Fluoride Thermal Energy Storage"; AFWAL TR-85-2063; 1985

19. Jacobson, D.L.; and Wang, J.H.; "Failure Analysis of a Sodium Inconel 617 Heat Pipe"; AFWAL TR-85-2064; 1985

20. Kaufman, W.B.; and Tower, L.K.; "Compatibility of Sodium and Lithium in Superalloy Heat Pipes"; AFWAL TR-85-2006; 1985

21. Lamp, T.R.; "Manufacturing Processes for Sodium/Inconel 617 Heat Pipes Report #1"; 1980

22. McKisson; et al; "Solubility Studies of Ultra Pure Transition Elements in Ultra Pure Alkali Metals"; NASA CR-10; October 1966

23. Soenen, M.; "Compatibility of Different Brazing Alloys During Long Time-Exposure in Sodium Loop";

24. Weatherford; Tyler; and Ku; WADD Technical Report 61-96; SWRI; 1961

25. Winslow, P.M.; "Ion Engine Reliability as Affected by Corrosion of Materials"; AIAA Electric Propulsion; 1963

26. Yamamoto, T.; and Tanaka, Y.; "Long-Term Operation Test of Sodium Heat Pipe";

27. Yamamoto, T.; Tanaka, Y.; Sasaki, M.; and Hatori, H.; "Study on life of Sodium Heat Pipe;

REPORT DOCUMENTATION PAGE

Form Approved
OMB No. 0704-0188

1. AGENCY USE ONLY *(Leave blank)*	2. REPORT DATE	3. REPORT TYPE AND DATES COVERED
	JULY 1992	Final Contractor Report

4. TITLE AND SUBTITLE

Materials Technology for Stirling Space Power Converters

5. FUNDING NUMBERS

WU-590-13-11
C-NAS3-26065

6. AUTHOR(S)

W. Baggenstoss
D. Mittendorf

7. PERFORMING ORGANIZATION NAME(S) AND ADDRESS(ES)

Allied-Signal Aerospace Company
Garrett Fluid Systems Division
1300 W. Warner Road
Tempe, Arizona 85284

8. PERFORMING ORGANIZATION REPORT NUMBER

41-11386

9. SPONSORING/MONITORING AGENCY NAMES(S) AND ADDRESS(ES)

National Aeronautics and Space Administration
Lewis Research Center
Cleveland, Ohio 44135-3191

10. SPONSORING/MONITORING AGENCY REPORT NUMBER

NASA CR-189102

11. SUPPLEMENTARY NOTES

Project Manager, Lanny G. Thieme, Power Technology Division, NASA Lewis Research Center

BUTION CODE

Date for general release July 1994

Subject Category 20

13. ABSTRACT *(Maximum 200 words)*

This program on Materials Technology for Stirling Space Power Converters was conducted in support of the NASA Lewis Research Center development of the Stirling power converter (SPC) for space power applications. The objectives of this contract were 1) to perform a technology review and analyses to support the evaluation of materials issues for the SPC; 2) to evaluate liquid metal compatibility issues of the SPC; 3) to evaluate and define a transient liquid phase diffusion bonding (TLPDB) process for the SPC joints to the Udimet 720 heater head; and 4) to evaluate alternative (to the TLPDB) joining techniques.

In the technology review, several aspects of the current Stirling design were examined including the power converter assembly process, materials joining, gas bearings, and heat exchangers. The supporting analyses included GLIMPS power converter simulation in support of the materials studies, and system level analysis in support of the technology review. The liquid metal compatibility study evaluated the use of liquid lithium, liquid sodium, and liquid NaK in the Stirling power converter. The TLPDB study developed specific TLPDB process parameters for use in the Stirling power converter. The alternative joining techniques study looked at the applicability of various joining techniques to the Stirling power converter requirements.

14. SUBJECT TERMS

Stirling engines
Superalloys
Udiment alloys
Diffusion bonding
Liquid metals

15. NUMBER OF PAGES

70

16. PRICE CODE

A04

17. SECURITY CLASSIFICATION OF REPORT	18. SECURITY CLASSIFICATION OF THIS PAGE	19. SECURITY CLASSIFICATION OF ABSTRACT	20. LIMITATION OF ABSTRACT
Unclassified	Unclassified	Unclassified	